STEADY STATE EVOLUTION OF DEBRIS DISKS AROUND A STARS

M. C. Wyatt
Institute of Astronomy, University of Cambridge, Madingley Road, Cambridge CB3 0HA, UK; wyatt@ast.cam.ac.uk

R. Smith
Institute for Astronomy, Royal Observatory, Blackford Hill, Edinburgh EH9 3HJ, UK

K. Y. L. Su and G. H. Rieke
Steward Observatory, University of Arizona, 933 North Cherry Avenue, Tucson, AZ 85721

J. S. Greaves
Scottish Universities Physics Alliance, University of St. Andrews, Physics and Astronomy, North Haugh, St. Andrews KY16 9SS, UK

and

C. A. Beichman[1] and G. Bryden
Jet Propulsion Laboratory, 4800 Oak Grove Drive, Pasadena, CA 91109

ABSTRACT

This paper confronts a simple analytical model for the steady state evolution of debris disks due to collisions with *Spitzer* observations of dust around main-sequence A stars. It is assumed that every star has a planetesimal belt, the initial mass and radius of which are drawn from distributions. In the model disk mass is constant until the largest planetesimals reach collisional equilibrium, whereupon mass falls $\propto t_{age}^{-1}$. We find that the detection statistics and trends seen at 24 and 70 μm can be fitted well by the model. While there is no need to invoke stochastic evolution or delayed stirring to explain the statistics, a moderate rate of stochastic events is not ruled out. Potentially anomalous systems are identified by a high dust luminosity compared with the maximum permissible in the model (HD 3003, HD 38678, HD 115892, HD 172555); their planetesimals may have unusual properties (high strength or low eccentricity), or this dust could be transient. The overall success of our model, which assumes planetesimals in all belts have the same strength, eccentricity, and maximum size, suggests the outcome of planet formation is reasonably uniform. The distribution of planetesimal belt radii, once corrected for detection bias, follows $N(r) \propto r^{-0.8 \pm 0.3}$ for 3–120 AU. Since belt boundaries may be attributed to unseen planets, this provides a unique constraint on A star planetary systems. It is also shown that P-R drag may sculpt the inner edges of A star disks close to the *Spitzer* detection threshold (HD 2262, HD 19356, HD 106591, HD 115892). This model can be readily applied to the interpretation of future surveys, and predictions for the upcoming SCUBA-2 survey include that 17% of A star disks should be detectable at 850 μm.

Subject headings: circumstellar matter — planetary systems: formation

1. INTRODUCTION

The asteroid and Kuiper belts lie in regions of the solar system that are stable over long timescales to the gravitational perturbations of the planets (Lecar et al. 2001). Dust produced in collisions between planetesimals in these belts inhabits a broader distribution, but one that is strongly influenced by the same gravitational perturbations (Dermott et al. 1994; Liou & Zook 1999; Moro-Martín & Malhotra 2003). These belts are thought to have started off with more than 200 times their present mass (Stern 1996; Bottke et al. 2005), and it is speculated that the belts were depleted in the same event that caused the late heavy bombardment (LHB). The LHB was a period of ~100 Myr duration that occurred 700 Myr after the solar system formed when the terrestrial planets were bombarded with a large influx of comets and asteroids, possibly due to restructuring of the planetary system in a dynamical instability (Gomes et al. 2005). The evolution of these planetesimal belts since this event is thought to have been relatively slow, with mass falling off due to collisional processing, but with large spikes in the dust content of the inner solar system occurring when two large asteroids collided (Nesvorný et al. 2003; Farley et al. 2006). Knowledge of the planetesimal and dust content of the solar system and how it evolves thus provides a rich source of information about both the planetesimals themselves and the planetary system in which they reside.

It is important to determine the evolution of the planetesimal belts around other stars, since this may be equally illuminating as to the nature and evolution of their planetary systems. Surveys have been undertaken to determine this evolution by measuring the infrared flux from dust produced in the collisional destruction of those planetesimals (Aumann et al. 1984). The observations are used to derive basic properties of the dust belts, such as their infrared luminosity L_{ir} (quoted as fractional luminosity, $f = L_{ir}/L_\star$) and the distance of the dust from the star (which is either the same as, or strongly dependent on, the planetesimal belt radius r), and these are then compared with stellar properties, such as age and spectral type. Most studies have focussed on the evolution of dust luminosity, showing that fractional luminosity decreases with age; e.g., Spangler et al. (2001) found the mean dust luminosity of disks of similar age falls off $\propto t^{-1.8}$, while Greaves & Wyatt (2003) inferred from detection statistics that the mass falls off $\propto t^{-0.5}$, Najita & Williams (2005) found the mass of the detected disks falls off $\propto t^{-1}$, and the upper limit

[1] Michelson Science Center, California Institute of Technology, Mail Stop 100-22, Pasadena, CA 91125.

in 24 μm of the A star disks was found to fall off $\propto t^{-1}$ (Rieke et al. 2005), while disk mass from far-IR statistics was inferred to be relatively age independent in the range 30–1000 Myr (Rhee et al. 2007). These results are thus in general agreement with the results of theoretical models, which show that a planetesimal belt evolving in quasi–steady state would lose mass due to collisional grinding down, giving a disk mass (and dust luminosity) that falls off $\propto t^{-1}$ (Dominik & Decin 2003; Wyatt et al. 2007).

However, Decin et al. (2003) noted that the maximum luminosity of debris disks remains constant at $f \approx 10^{-3}$ even for the oldest stars, and this was explained by Dominik & Decin (2003) as a consequence of delayed stirring, in which dust is not produced in the planetesimal belt until Pluto-sized objects form and ignite a collisional cascade. Since planet formation models predict that such massive bodies take longer to form farther from the star (Kenyon & Bromley 2004), that interpretation makes the prediction that the radius of the belts should increase with stellar age, and more recent surveys have also considered the evolution of radius. While in submillimeter surveys there is as yet no evidence of any evolution of radius with age (Najita & Williams 2005; Williams & Andrews 2006), the latest far-IR results for A stars do appear to show some evidence that radius is increasing with age, based on the fact that excess emission is detected at much later ages at 70 μm than at 24 μm (Su et al. 2006).

It has also been suggested that much of the dust we see in some systems is produced episodically in collisions between large planetesimals, much in the same way dust in the zodiacal cloud increases when collisions occur in the asteroid belt, and that such collisions contribute to the large spread in the infrared luminosities seen in disks around A stars of similar age (Rieke et al. 2005). This scenario is supported by the discovery of a population of dust grains around Vega in the process of removal by radiation pressure, which indicates that this system cannot have remained in steady state for the full 350 Myr age of the star (Su et al. 2005). More recently, it has also been shown that the few Sun-like stars with hot dust at a few AU (Gaidos 1999; Beichman et al. 2005; Song et al. 2005; Wyatt et al. 2005) must be transient, since they are too bright for their age to be planetesimal belts that have evolved due to steady state collisional processing; such systems may be undergoing periods analogous to the LHB in the solar system (Wyatt et al. 2007). A stochastic element to disk evolution would introduce additional free parameters in models and would complicate interpretation of the observed statistics if it plays a major role.

It has thus not yet been possible to arrive at a consistent picture for debris disk evolution. The fact that surveys are undertaken for different spectral types, at different wavelengths, with different sensitivities to detections, has also added confusion to the interpretation of the statistics. In this paper we revisit a simple analytical model for the steady state collisional evolution of planetesimal belts that was originally explored in Dominik & Decin (2003) and recast with slightly modified assumptions in Wyatt et al. (2007). This model, including how it is applied in this paper to populations of debris disks, is given in § 2. In § 3 we build a model for the population of disks around A stars which is constrained using the 24 μm statistics presented in Rieke et al. (2005). The properties of the model population are then compared in § 4 with those of the A star disks detected in surveys at 70 μm (Su et al. 2006) and the model parameters are fine tuned. These results indicate that, with the exception of a few outlier systems, the available statistics can be fitted by steady state collisional evolution without having to invoke a major role for stochasticity or delayed stirring. Finally, the model population is used to make

predictions for future debris disk surveys in the submillimeter (§ 5). The conclusions are given in § 6.

2. DEBRIS DISK POPULATION MODEL

This section describes the simple analytical model for the steady state collisional evolution of planetesimal belts that was derived in Wyatt et al. (2007) (§ 2.1), and illustrates how that model is applied in this paper to populations of debris disks (§ 2.2).

2.1. Steady State Collisional Evolution

The planetesimal belt is assumed to be in collisional equilibrium with a size distribution defined by

$$n(D) = KD^{2-3q}, \tag{1}$$

where q is 11/6 for an infinite collisional cascade (Dohnanyi 1969), and D is the diameter of the planetesimals in km. That distribution is assumed to hold from the largest planetesimal in the disk, of diameter D_c (in km), down to the size below which particles are blown out by radiation pressure as soon as they are created, D_{bl} (in μm). If q is in the range 5/3 to 2, then most of the mass is in the largest planetesimals while the cross-sectional area is dominated by the smallest particles such that for spherical particles of density ρ in kg m^{-3}:

$$\sigma_{tot} = 3.5 \times 10^{-17} K (3q-5)^{-1} \left(10^{-9} D_{bl}\right)^{5-3q}, \tag{2}$$

$$M_{tot} = 2.5 \times 10^{-9} (3q-5)(6-3q)^{-1} \rho \sigma_{tot} D_{bl} \left(10^9 D_c/D_{bl}\right)^{6-3q}, \tag{3}$$

where σ_{tot} is in AU^2, M_{tot} is in $M_\oplus$, and the rest of the units are as described above and are used consistently throughout the paper.

The planetesimal belt is assumed to be at a radius r, and have a width dr, both in units of AU. Assuming that the grains act like blackbodies, and so absorb all the radiation they intercept, the fractional luminosity, $f = L_{ir}/L_\star$, of the dust emission is given by

$$f = \sigma_{tot}/(4\pi r^2). \tag{4}$$

In other words, in this model σ_{tot}, M_{tot}, and f are all proportional to each other and just one is needed to define the scaling factor K in equation (1).

Assuming the particles act like blackbodies also allows us to write down some other simple relations:

$$D_{bl} = 0.8(L_\star/M_\star)(2700/\rho), \tag{5}$$

where $L_\star$ and $M_\star$ are in solar units. Also the emission from the disk at a wavelength λ is given by

$$F_{\nu disk} = 2.35 \times 10^{-11} B_\nu(\lambda, \ T)\sigma_{tot} d^{-2}, \tag{6}$$

where d is the distance to the star in pc, giving F_ν in Jy if the Planck function B_ν is in Jy sr^{-1}. The dust temperature can be worked out from

$$T = 278.3 L_\star^{0.25} r^{-0.5} \tag{7}$$

in K. The emission from the star at the same wavelength is given by

$$F_{\nu\star} = 1.77 B_\nu(\lambda, \; T_\star) L_\star T_\star^{-4} d^{-2}, \qquad (8)$$

where $T_\star$ is in K.

In a collisional cascade the amount of material within a given size range D to $D + dD$ decreases as these planetesimals are destroyed in collisions with other members of the cascade, but is replaced at the same rate by fragments created from the collisional destruction of larger objects. The long-timescale evolution is thus determined by the removal of mass from the top end of the cascade. In this model the scaling factor K (and so the total mass and fractional luminosity) decreases as the number of planetesimals of size D_c decreases. The loss rate of such planetesimals is determined by their collisional lifetime, which was derived in Wyatt et al. (2007) to be

$$t_c = \left[\frac{3.8\rho r^{3.5}(dr/r)D_c}{M_\star^{0.5}M_{\text{tot}}}\right]\left\{\frac{(12q-20)\left[1+1.25(e/I)^2\right]^{-0.5}}{(18-9q)G(q,\;X_c)}\right\} \qquad (9)$$

in Myr, where e and I are the mean eccentricities and inclinations of the planetesimals' orbits, and the factor $G(q,\;X_c)$ is given by

$$G(q,\;X_c) = \left[\left(X_c^{5-3q}-1\right) + (6q-10)(3q-4)^{-1}\left(X_c^{4-3q}-1\right) \right.$$
$$\left. + (3q-5)(3q-3)^{-1}\left(X_c^{3-3q}-1\right)\right], \qquad (10)$$

and $X_c = D_{cc}/D_c$, where D_{cc} is the smallest planetesimal that has enough energy to catastrophically destroy a planetesimal of size D_c. The factor X_c can be worked out from the dispersal threshold, $Q_D^\star$, defined as the specific incident energy required to catastrophically destroy a particle such that (Wyatt & Dent 2002)

$$X_c = 1.3 \times 10^{-3}\left(\frac{Q_D^\star r M_\star^{-1}}{1.25e^2+I^2}\right)^{1/3}, \qquad (11)$$

where $Q_D^\star$ is in J kg^{-1}.

Assuming that collisions are the only process affecting the evolution of the disk mass $M_{\text{tot}}(t)$, then that mass (or equivalently for K, σ_{tot}, or f) can be worked out by solving $dM_{\text{tot}}/dt = -M_{\text{tot}}/t_c$ to give

$$M_{\text{tot}}(t) = M_{\text{tot}}(0)/[1 + t/t_c(0)], \qquad (12)$$

where $M_{\text{tot}}(0)$ is the initial disk mass and $t_c(0)$ is the collisional lifetime at that initial epoch; this solution is valid as long as mass is the only time-variable property of the disk. This results in a disk mass that is constant at $M_{\text{tot}}(0)$ for $t \ll t_c(0)$, but that falls off $\propto t^{-1}$ for $t \gg t_c(0)$.

As noted in Wyatt et al. (2007), one property of this evolution is that, since the expression for $t_c(0)$ includes a dependence on $M_{\text{tot}}(0)$, the disk mass at late times is independent of initial disk mass. This is because more massive disks process their mass

faster. This means that for any given age, t_{age}, there is a maximum disk mass M_{max} (and also infrared luminosity, f_{max}) that can remain due to collisional processing:

$$M_{\text{max}} = \left[\frac{3.8\times10^{-6}\rho r^{3.5}(dr/r)D_c}{M_\star^{0.5}t_{\text{age}}}\right]$$
$$\times\left\{\frac{(12q-20)\left[1+1.25(e/I)^2\right]^{-0.5}}{(18-9q)G(q,\;X_c)}\right\}, \qquad (13)$$

$$f_{\text{max}} = \left[\frac{10^{-6}r^{1.5}(dr/r)}{4\pi M_\star^{0.5}t_{\text{age}}}\right]\left\{\frac{2\left[1+1.25(e/I)^2\right]^{-0.5}}{G(q,\;X_c)}\right\}\left(\frac{D_{\text{bl}}}{D_c}\right)^{5-3q}, \qquad (14)$$

where again this mass is in units of $M_\oplus$.

2.2. Application to Populations of Debris Disks

To apply this evolution to populations of debris disks, the following assumptions were made. All stars have a planetesimal belt that is undergoing a collisional cascade (although this is not necessarily detectable). The initial conditions of these belts are as described in § 2.1 using the parameters $M_{\text{tot}}(0)$, r, dr, ρ, D_c, D_{bl} (which is defined by $L_\star$ and $M_\star$), and q. The subsequent evolution is determined by $Q_D^\star$, e and I (§ 2.1). To simplify the problem we set $I = e$, $\rho = 2700$ kg m^{-3}, $dr = r/2$, and $q = 11/6$ for all disks and did not consider the effects of changing these parameters. The parameters $Q_D^\star$, e, and D_c were assumed to be the same for all disks, and their values were constrained by a fit to the observed properties of the known disks; the consequence of choosing different values is discussed. The remaining parameters, $M_{\text{tot}}(0)$, r, $L_\star$, and $M_\star$ were chosen from distributions for a population of a large number of disks (10,000 in this case).

For each disk the stellar spectral type was chosen at random from the appropriate range (i.e., B8–A9 for comparison with the sample of Rieke et al. 2005), thus defining $L_\star$, $M_\star$, and so D_{bl}. The distribution of initial disk masses, $M_{\text{tot}}(0)$, was based on the results of Andrews & Williams (2005), who did a submillimeter study of protoplanetary disks in the Taurus-Auriga star forming region, i.e., for $\sim$1 $M_\odot$ stars, from which they derived that this population has a lognormal distribution of dust masses that is centered on $M_{\text{mid}} = 3.3\ M_\oplus$ and has a 1 σ width of 1.14 dex. We used the same distribution but allowed M_{mid} to be different from that found in Taurus-Auriga, and this was a free parameter. For the distribution of disk radii, a power-law distribution $N(r) \propto r^\gamma$ in the range 3–120 AU was adopted, where $N(r)dr$ is the number of disks with radii in the range r to $r + dr$. The range 3–120 AU was chosen from the range of radii inferred for the sample of 46 A star disks with radius estimates (Table 1), and the exponent γ was determined from a fit to the observations. The mass evolution of each disk was then completely defined using equations (9) and (12), and its properties at the current epoch were determined by assigning an age, t_{age}, randomly from the appropriate range (i.e., 0–800 Myr for A stars). The stars were also assigned a random distance in the range 0–45 pc assuming an isotropic distribution [i.e., $N(d) \propto d^2$]; given that there are $\sim$100 A stars within 45 pc, the model is overpopulated by a factor of around 100 compared with the real population (although note that distance only becomes important in this paper in § 5).

TABLE 1

Main-Sequence A-Type Stars with Excess Emission Detected at 24 and 70 μm (or 25 and 60 μm)

Star Name	Spectral Type	$T_\star$ (K)	$M_\star$ ($M_\odot$)	$L_\star$ ($L_\odot$)	d (pc)	t_{age} (Myr)	$f = L_{ir}/L_\star$	r (AU)	f/f_{max}	f/f_{pr}
				Su et al. (2006) sources						
HD 2262	A7 V	9506	2.9	12.0	23.5	690	0.71×10^{-5}	28	1.0	0.9
HD 14055	A1 Vnn	9225	2.7	33.0	36.1	300	6.7×10^{-5}	79	0.65	15
HD 19356	B8 V	11939	3.8	347	28.5	300	0.32×10^{-5}	30	1.1	0.4
HD 27045	A3 m	8709	2.3	8.0	28.7	193	1.1×10^{-5}	22	0.49	1.3
HD 28355	A7 V	7852	1.8	18.0	49.2	625	5.6×10^{-5}	49	1.8	12
HD 30422	A3 IV	8709	2.3	9.0	57.5	10	4.9×10^{-5}	40	0.033	8.1
HD 31295	A0 V	9506	2.9	26.0	37.0	10	4.5×10^{-5}	78	0.014	9.3
HD 38056	A0 V	9506	2.9	54.0	132	250	4.8×10^{-5}	62	0.91	8.9
HD 38206	A0 V	9506	2.9	32.0	69.2	9	14×10^{-5}	59	0.078	25
HD 38678	A2 Vann	8974	2.5	16.0	21.5	231	9.8×10^{-5}	7	100	6.7
HD 39060	A5 V	8203	2.0	13.0	19.3	15	140×10^{-5}	24	5.0	200
HD 71043	A0 V	9506	2.9	31.0	73.1	11	4.7×10^{-5}	52	0.044	8.0
HD 71155.................	A0 V	9506	2.9	40.0	38.3	169	2.5×10^{-5}	44	0.58	3.9
HD 75416	B8 V	11939	3.8	111	96.9	8	4.7×10^{-5}	17	0.96	4.0
HD 79108	A0 V	9506	2.9	60.0	115	320	5.0×10^{-5}	77	0.76	10
HD 80950	A0 V	9506	2.9	39.0	80.8	80	7.5×10^{-5}	20	4.7	7.9
HD 95418	A1 V	9225	2.7	68.0	24.3	300	1.3×10^{-5}	47	0.55	2.1
HD 97633	A2 V	8974	2.5	141	54.5	550	0.71×10^{-5}	36	1.4	1.1
HD 102647	A3 V	8709	2.3	17.0	11.1	50	2.0×10^{-5}	21	0.40	2.4
HD 106591	A3 V	8709	2.3	26.0	25.0	300	0.50×10^{-5}	16	1.5	0.5
HD 110411................	A0 V	9506	2.9	23.0	36.9	10	3.7×10^{-5}	53	0.026	6.3
HD 111786................	A0 III	9506	2.9	22.0	60.2	200	3.0×10^{-5}	47	0.53	4.7
HD 115892................	A2 V	8974	2.5	26.0	18.0	350	1.1×10^{-5}	6	32	0.7
HD 125162	A0 p	9506	2.9	16.0	29.8	313	5.1×10^{-5}	42	1.6	7.7
HD 136246	A1 V	9225	2.7	31.0	144	15	4.8×10^{-5}	81	0.021	11
HD 139006	A0 V	9506	2.9	83.0	22.9	314	1.4×10^{-5}	45	0.85	2.3
HD 158460	A1 V	9225	2.7	105	104	260	0.53×10^{-5}	68	0.11	1.1
HD 161868	A0 V	9506	2.9	29.0	29.1	184	7.5×10^{-5}	64	0.72	14
HD 165459	A2 V	8974	2.5	13.0	89.3	5	4.7×10^{-5}	31	0.037	6.6
HD 172167	A0 V	9506	2.9	58.0	7.8	200	2.3×10^{-5}	114	0.093	5.8
HD 181296	A0 Vn	9506	2.9	22.0	47.7	30	20×10^{-5}	25	2.1	23
HD 183324	A0 V	9506	2.9	22.0	59.0	10	1.0×10^{-5}	51	0.008	1.8
HD 216956	A3 V	8709	2.3	18.0	7.7	200	6.1×10^{-5}	67	0.38	13
HD 221756	A1 III	9225	2.7	27.0	71.6	130	1.9×10^{-5}	50	0.21	3.3
HD 225200	A0 V	9506	2.9	47.0	129	90	8.0×10^{-5}	94	0.20	18
				Additional sources from literature						
HD 1438[a]	B8 V	11939	3.8	219	212	95	26×10^{-5}	114	1.1	57
HD 3003[b]....................	B8 V	9500	2.9	21.0	46.5	50	11×10^{-5}	7	32	6.7
HD 9672[a]	A1 V	9225	2.7	22.8	61.3	20	72×10^{-5}	68	0.54	140
HD 21997[b]	A3 IV/V	8750	1.9	14.4	73.8	50	47×10^{-5}	79	0.39	120
HD 109573[b]..............	A0 V	10000	2.9	24.3	67.1	8	330×10^{-5}	27	8.7	410
HD 110058[a]	A0 V	9506	2.9	10.0	99.9	10	140×10^{-5}	18	7.5	140
HD 141569[b]	B9.5 e	10500	3.1	24.2	99.0	5	460×10^{-5}	35	4.4	620
HD 153053[b]..............	A5 IV/V	8000	1.8	12.3	50.7	420	7.6×10^{-5}	49	1.4	16
HD 158352[b]..............	A8 V	7750	1.7	24.0	63.1	600	7.8×10^{-5}	82	0.85	22
HD 172555[b]..............	A5 IV/V	8000	2.0	9.5	29.2	12	51×10^{-5}	4	86	28
HD 176638[a]..............	B9.5 V	10000	3.1	47.3	56.3	200	7.7×10^{-5}	41	2.9	11

[a] Based on excess emission detected at 25 and 60 μm by *IRAS*.
[b] Based on excess emission detected at 24 and 70 μm by *Spitzer*.

The free parameters in this population model are thus M_{mid}, γ, D_c, e, and $Q_D^\star$.

3. A STAR POPULATION MODEL: FIT TO 24 μm STATISTICS

Here the debris disk population model of § 2 is applied to the statistics of the incidence of disks around A stars presented in Rieke et al. (2005) based on observations at 24 μm. There are two main aims. The first, which is described in the rest of this section, is to determine whether these statistics can be reproduced with steady state evolution of the disks, and if so to set constraints on the physical properties and starting conditions of the disks in that population. The second is to use the resulting model population to make predictions for the properties of A star disks found in surveys at other wavelengths and to determine whether this simple model can explain the trends seen in the data. This is described in §§ 4 and 5, where the model parameters are also fine tuned.

3.1. *Rieke et al. (2005) Sample*

Rieke et al. (2005) searched a sample of 76 individual main-sequence A stars and a number of young stellar clusters for excess 24 μm emission above photospheric levels using *Spitzer* and combined the data with archival results from *IRAS* for a total sample size of 266 A stars. They also determined the ages of all stars in a consistent manner, thus providing a very useful sample from which to study the evolution of debris around A stars. Their main result was a plot of $F_{24tot}/F_{24\star}$ versus age for all objects which showed a decrease in the upper envelope $\sim$150 Myr/t_{age} (see Fig. 1). The statistics were further quantified by splitting the sample into three age bins (<90, 90–189, and >190 Myr), and classifying sources as either having small excess ($F_{24tot}/F_{24\star} <$ 1.25), medium excess ($1.25 < F_{24tot}/F_{24\star} < 2$), or large excess ($F_{24tot}/F_{24\star} > 2$; see their Fig. 3 and our Fig. 1, *middle*). Data on 12 objects was also presented at 70 μm (see their Fig. 2 and our Fig. 1, *bottom*, for a different version of this data).

3.2. *Best-Fit Model Population*

Our best-fit model for the disks around a population of 10,000 main-sequence A stars is shown in Figure 1. For each disk the stellar spectral type was chosen at random from the range B8 V–A9 V, with the ages of the disks chosen randomly from the range 0−800 Myr (that of the stars in the Rieke et al. sample). All disks were assumed to have physical properties corresponding to $Q_D^\star = 300$ J kg^{-1}, $e = 0.05$, and $D_c = 60$ km. The distribution of their initial masses had $M_{mid} = 10 M_\oplus$, slightly higher than that inferred for the disks of Sun-like stars in Taurus-Auriga to account for a slightly higher disk mass expected around more massive stars (Natta et al. 2000). The consequence of choosing different values is discussed in § 3.3.

The distribution of radii was constrained using the 12 disks with data at 24 and 70 μm in Rieke et al. (2005). Their values of F_{70disk}/F_{24disk} were converted into dust temperature and then radii (both assuming blackbody emission) to derive a distribution of radii that is reasonably flat, falling off only slowly between 3 and 120 AU (Fig. 1, *bottom*). While this sample is small, this distribution compares well with the distribution of radii inferred by Najita & Williams (2005) from their submillimeter sample of main-sequence stars, and with that inferred from the larger sample of 46 A star disks for which radii could be estimated, which is discussed in § 4 (see Fig. 3). It is important to account for the fact that this sample of stars with estimated radii is not representative of the whole population, since it only includes disks that can be detected at 24 and 70 μm. For this reason the observed distribution of radii was not compared with the power-law distribution used as input to the model, but with the subsample of disks in the model population that could have been detected at both 24 and 70 μm, which was assumed to be those with $F_{24tot}/F_{24\star} > 1.1$ and $F_{70tot}/F_{70\star} > 1.55$ (Fig. 1, *bottom*). The exponent in the power-law distribution was found to be $\gamma \approx -0.8 \pm 0.6$, with relatively poor constraints due to the small sample size.

One immediately clear result is that the observed statistics can be well fitted using the model with a realistic set of planetesimal belt parameters (i.e., those given above) and with an initial mass distribution consistent with that inferred for protoplanetary disks. Thus, there is no requirement for disk flux to have any stochastic component to its evolution to explain the Rieke et al. (2005) statistics, although this does not mean that stochasticity cannot play a role in determining the observable properties of the disks. The large spread in infrared excess for stars at any given age arises in the model from the distribution of their initial starting
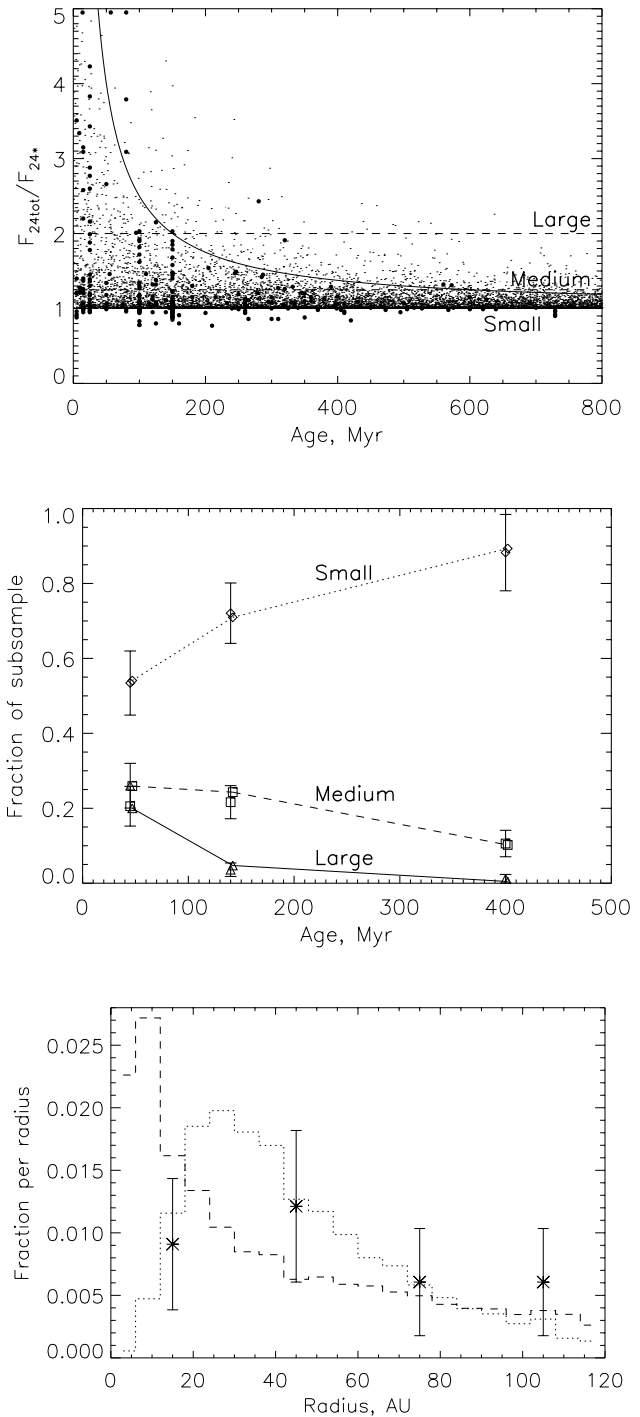

Fig. 1.—Fit of the debris disk population model to the results of Rieke et al. (2005) (§ 3). The model is comprised of 10,000 planetesimal belts with initial masses chosen from a lognormal distribution centered on 10 $M_\oplus$, radii in the range 3–120 AU (power-law exponent $\gamma = -0.8$), around stars of spectral types B8–A9 and ages 0−800 Myr. *Top*: Total 24 μm flux divided by that of the stellar photosphere (cf. Fig. 1 of Rieke et al. 2005). The model population is shown with dots, and the disk observations of Rieke et al. (2005) are shown with filled circles. The upper limit inferred from statistics in Rieke et al. (2005), $F_{24disk}/F_{24\star} \approx 150 t_{age}^{-1}$, is shown with a solid line. *Middle*: Fraction of stars with flux ratios in the different age bins used by Rieke et al. (2005) for their Fig. 3 (<90 Myr, 90–189 Myr, >190 Myr): $F_{24tot}/F_{24\star} = 1$–1.25 (diamonds = small excess), 1.25–2 (squares = medium excess), >2 (triangles = large excess). Observed values are shown with $\sqrt{N}$ error bars, and model values are joined with dotted, dashed, and solid lines for increasing $F_{24tot}/F_{24\star}$. *Bottom*: Distribution of radii in the model (dashed line is the whole population, dotted line is those predicted to be detectable at 24 and 70 μm) compared with the distribution inferred from observations in Rieke et al. (2005) with $\sqrt{N}$ error bars (*asterisks*). The *y*-axis is the fraction of disks in each sample that fall in the different radius bins (of width 6 or 30 AU).

masses, as well as from that of their radii, and to a lesser extent from the spectral type of the parent star. Disks of high 24 μm flux in the model are those with high initial disk masses and with radii that are larger than average, since rapid collisional processing means that close-in planetesimal belts tend to have low luminosities, except at the youngest ages. The model also predicts that disks of high 24 μm flux should be found predominantly around higher luminosity stars; e.g., 40% of the stars in the model with $F_{24tot}/F_{24\star} > 2$ are A0 or earlier, compared with 25% of stars in the whole population. We have not been able to confirm this trend in the Rieke et al. (2005) data, for which any evidence of a change in excess ratio with spectral type is overwhelmed by the strong age dependence of this parameter.

3.3. Constraints and Flexibility in Model Parameters

The model parameters described in § 3.2 are not uniquely constrained in the formulation of the evolution described in § 2:

1. The upper envelope in the model population in Figure 1 (*top*) is determined by f_{max} given in equation (14). Thus, given the parameters and distributions that are fixed in the model, the upper envelope seen in Figure 1 (*top*) in both the model and observed populations would be reproduced by any combination of parameters with the same $D_c^{3q-5}/G(q, X_c)$. This means that if $q = 11/6$ and $X_c \ll 1$, then the same statistics are reproduced as long as

$$D_c^{1/2}Q_D^{\star 5/6}e^{-5/3} \approx 130 \times 10^3. \quad (15)$$

The parameters dr/r, ρ, e/I, and q could be changed and accounted for by modifying the other variables in a similar manner. The factor derived here for A stars in equation (15) is 4 times lower than that used in Wyatt et al. (2007) to assess whether the hot dust of Sun-like stars exceeds the maximum possible for steady state planetesimal belts, indicating that the limit used in that paper is, if anything, too stringent (although it is possible that the properties of the planetesimal belts of a population of Sun-like stars are different from those of A stars given in eq. [15]).

2. The mass distribution in the model determines the path of each disk under the upper envelope described above. This mass distribution thus determines the fraction of disks that end up in the different bins of $F_{24tot}/F_{24\star}$ at different times. If the relation given in equation (15) holds, then the same statistics as the model shown in Figure 1 would also be reproduced with a disk mass distribution which is given by

$$M_{mid}D_c^{-0.5} \approx 1.3, \quad (16)$$

since, from equation (9), this would result in the same distribution of t_c.

In other words, if a maximum planetesimal size of 2000 km had been assumed, the disk mass distribution would have to be centered on $M_{mid} = 60 \, M_\oplus$, i.e., close to an order of magnitude higher than that inferred from the distribution of protoplanetary disks including nondetections (Andrews & Williams 2005), but half the mean mass of disks detected around Herbig Ae stars (Natta et al. 2000). In such an interpretation equation (15) indicates that $e \approx 0.008\sqrt{Q_D^\star}$, and so is satisfied by $e = 0.1$ and $Q_D^\star = 140$ J kg^{-1}.

Distributions with more massive disks are possible by assuming, e.g., that some fraction of stars end up with only very tenuous disks (which are not detected at 24 μm). Lower mean disk masses are also possible to accommodate by reducing the maximum planetesimal size and planetesimal eccentricity; e.g., the statistics are also reproduced with $M_{mid} = 1 \, M_\oplus$, $D_c = 0.6$ km, $e = 0.013$, $Q_D^\star = 300$ J kg^{-1}. It is not possible to differentiate among these possibilities at this stage. Both atypically high and low starting masses for debris disks have been suggested by other studies: e.g., a jump down in disk mass by a factor of 10–100 is inferred when extrapolating the masses of the known debris disks back in time and comparing with protoplanetary disk masses (Wyatt et al. 2003), and the statistics of the incidence of Sun-like stars with planets and debris suggest that it is stars with disks with $\sim$20 $M_\oplus$ of solid material (i.e., those with masses 6 times higher than M_{mid}) that end up with detectable debris (Greaves et al. 2007). It may also be reasonable to assume that only some fraction of the initial disk mass ends up in the planetesimal belt, the remainder being incorporated into planets or in some other way removed.

The radius distribution is also particularly poorly constrained at present. On top of the large uncertainty in the power-law exponent γ, it is also possible that the range of radii for the planetesimal belts is broader than that assumed here (3–120 AU). The model predicts that planetesimal belts that fall outside this range would not be detected in a 24 μm survey such as that of Rieke et al. (2005), since the rapid collisional processing of those <3 AU means that these belts fall below the detection threshold soon after they form, while those >120 AU would be too cold for their emission at 24 μm to be detectable above the photosphere. Thus, we cannot rule out the existence of such close-in or far-out planetesimal belts around up to 40% of A stars from this study.

It is also important to point out that while the model presented here considered disks that all had the same maximum planetesimal size but with a range of starting masses, a model with a narrower distribution of initial masses and a distribution of maximum planetesimal sizes could also fit the observations. Likewise, the model chose to set planetesimal strength, eccentricity, and maximum size to be the same for all systems. It is not a conclusion that this has to be the case, since a population for which these parameters are chosen from distributions can also fit the data. In that instance the properties of the planetesimal belts would also contribute to the spread in infrared excess seen at any given age.

In conclusion, the statistics can be readily reproduced with a population of disks with reasonable starting parameters without recourse to stochastic evolution models. The possibility remains, however, that some fraction of the disks in the Rieke et al. (2005) sample are undergoing transient events. For example, some of the disks may exceed the maximum luminosity permitted for disks at their observed radius and age. This limit is given in equation (14) and was used in Wyatt et al. (2007) to show that several of the disks found <10 AU around Sun-like stars must be transient. One system in the Rieke et al. (2005) sample that is close to this limit is ζ Lep (HD 38678), a 230 Myr A2 V star which has dust with an infrared luminosity $f = 10 \times 10^{-5}$ (Chen & Jura 2001; Su et al. 2006), predicted to lie at $\sim$7 AU based on its 24 and 70 μm fluxes, and found to have a resolved size of $\sim$3 AU at 18 μm, with emission spread across the range 2–8 AU (Moerchen et al. 2007). For dust at 7 AU f_{max} is 0.16×10^{-5} using the parameters inferred above for the rest of the A star sample (see also Table 1); i.e., this system is close to the limit at which we would infer it must be transient, which was considered in Wyatt et al. (2007) to be when $f > 100f_{max}$. Further, some fraction of the disks could have a

two-component structure, e.g., like the F2 V star η Corvi, which has dust at $\sim$1.5 AU that is inferred to be transient (Wyatt et al. 2007), as well as at 150 AU (Wyatt et al. 2005), which is likely to be in steady state. Indeed, it has recently been shown that Vega (HD 172167) does have an additional dust component at a few AU (Absil et al. 2006), as was already inferred for HR 4796 (HD 109573; Augereau et al. 1999). Also, there could be a stochastic element to the mid-IR emission which is not present in the far-IR emission, such as has been inferred for Vega based on the fact that the mid-IR emission seems to be dominated by grains undergoing blow out by radiation pressure (Su et al. 2005). Detailed study of individual objects is required to resolve these uncertainties on a case-by-case basis. Since the threshold for detection of a stochastic event is high with the current observations, it is likely that the number of such cases is underestimated. Nonetheless, the correspondence of the time decay of the excesses with a simple model of steady state evolution that has few free parameters suggests that stochastic events do not dominate the behavior.

3.4. *Interpretation of Model Parameters*

Given the degeneracy in the model parameters described in § 3.3, it is not worth dwelling on a specific interpretation of the values used in the best fit model of § 3.2, except to say that these are reasonable parameters based on models of planetesimal strength (Benz & Asphaug 1999) and of planet formation processes (Kenyon & Bromley 2002). A more detailed collisional evolution model would be required to ascertain what this is telling us about the physical properties of the planetesimals, for example. The important point is that the observed statistics can be explained by a model population in which the evolution of individual disks is very simple and behaves in the manner described in § 2.

4. EXPLAINING 24 AND 70 μm A STAR RESULTS

While there is still uncertainty in how accurately the simple collisional evolution model of § 2.1 follows the evolution of individual disks (e.g., the validity of a single power-law size distribution; see Wyatt et al. 2007), the results of § 3 show that the debris disk population model based on that evolution can reproduce the 24 μm statistics well. In this section, the model population is further tested by comparing its predictions for the surveys at 70 μm with the statistics observed by Su et al. (2006) (§ 4.1). The model parameters are also fine tuned in this section to provide a better fit to the observed statistics from that paper. By plotting the model population in different ways, we are able to provide a qualitative explanation of the trends seen in this survey, and to reproduce the properties of a sample of 46 A stars for which excess emission has been detected at both 24 and 70 μm and so for which estimates for the radii of their planetesimal belts can be made (§ 4.2). These plots provide a framework that can be used to interpret the statistics of surveys at other wavelengths and to understand the implications of different detection thresholds.

4.1. *Fit to Su et al. (2006)* 70 μm *Statistics*

The Rieke et al. (2005) 24 μm survey of A stars for excess emission described in § 3.1 has recently been extended to 70 μm and the results presented in Su et al. (2006). In that paper a sample of $\sim$160 main-sequence A-type stars (spectral types B6–A7) were searched for excesses at both 24 and 70 μm using *Spitzer*, and ages were assigned to these stars using a consistent scheme. This sample was then supplemented with a further 19 stars with *IRAS* data at 25 and 60 μm. In addition to reproducing the results

for the evolution of 24 μm excesses around A stars found by Rieke et al. (2005; e.g., Fig. 1), the main new result of Su et al. (2006) was comparable plots for the evolution of 70 μm excesses. Plots of $F_{\rm tot}/F_{\star}$ against $t_{\rm age}$ for both 24 and 70 μm (Figs. 4 and 5 of Su et al. 2006) and the fraction of stars in different age bins that have small excess ($F_{\rm 24tot}/F_{24\star} < 1.25$, $F_{\rm 70tot}/F_{70\star} < 5$), medium excess ($1.25 < F_{\rm 24tot}/F_{24\star} < 2$, $5 < F_{\rm 70tot}/F_{70\star} < 20$), and large excess ($F_{\rm 24tot}/F_{24\star} > 2$, $F_{\rm 70tot}/F_{70\star} > 20$; Fig. 9 of Su et al. 2006) are shown in Figure 2. The observations show that while 70 μm excesses are also characterized by a $t_{\rm age}^{-1}$ falloff, the disk emission persists much longer, and at much higher levels relative to the photospheric flux, than at 24 μm. Su et al. (2006) also identified samples of stars for which excess emission was detected at both 24 and 70 μm (group I sources in Su et al.), or at 70 but not 24 μm (group II sources in Su et al.), or at 24 but not 70 μm (group V sources in Su et al.).

The model of § 3 was fitted to the distribution of disk properties above the 24 μm threshold, and the only way 70 μm information was included in the model fit was through the 12 disks with 70 μm detections in Rieke et al. (2005), which set rather loose constraints on the exponent in the power-law distribution of planetesimal belt radii (Fig. 1, *bottom*). In fact, it turns out that the 70 μm statistics of Su et al. (2006) are fitted extremely well using exactly the same model population. However, we used the new distributions of 24 and 70 μm excesses as a function of age shown in Figure 2, and the distribution of radii for the 46 A star disks that have been detected at 24 and 70 μm (see § 4.2 and Fig. 3), to set new constraints on the model parameters. Figures 2 and 3 show the resulting best-fit model population and illustrate how the model reproduces the longer timescale for the decay of 70 μm excesses seen by Su et al. (2006), and not just in a qualitative way; the model reproduces the observed statistics very well at 70 μm, just as it does at 24 μm. While the upper envelope in Figure 2 (*top right*) is around 5 times as high as that of the observed disks at any given age, this can be attributed to small number statistics, since the observed upper envelope would increase as more stars are included in the sample, and indeed the upper envelope in the model population is close to that observed when the number of stars included is comparable with the observed population (i.e., 2 orders of magnitude fewer stars in the model population than shown in Fig. 2).

The parameters derived from this fit are almost completely unchanged from those derived in § 3, with the only change being in the planetesimal strength to $Q_D^{\star} = 150$ J kg^{-1}. This means that the statistics can equally be fitted by any combination of parameters:

$$D_c^{1/2} Q_D^{\star 5/6} e^{-5/3} \approx 74 \times 10^3, \qquad (17)$$

which now supersedes equation (15), while the combination of parameters required to fit the statistics that is given in equation (16) remains unchanged. The exponent in the radius distribution also remains unchanged as a result of the new fit, but this distribution is now better constrained to $N(r) \propto r^{-0.8 \pm 0.3}$.

4.2. *Comparison with Disks Detected at* 24 *and* 70 μm

In addition to the quantitative results on the incidence of disks of different levels of excess seen around stars of different ages, Su et al. (2006) identified several trends in their data which also require explanation in terms of the model. These include: (1) disks with excess at 70 μm but not 24 μm have lower fractional luminosities than those detected at both 24 and 70 μm; (2) stars that have excesses at 70 μm but not at 24 μm are on
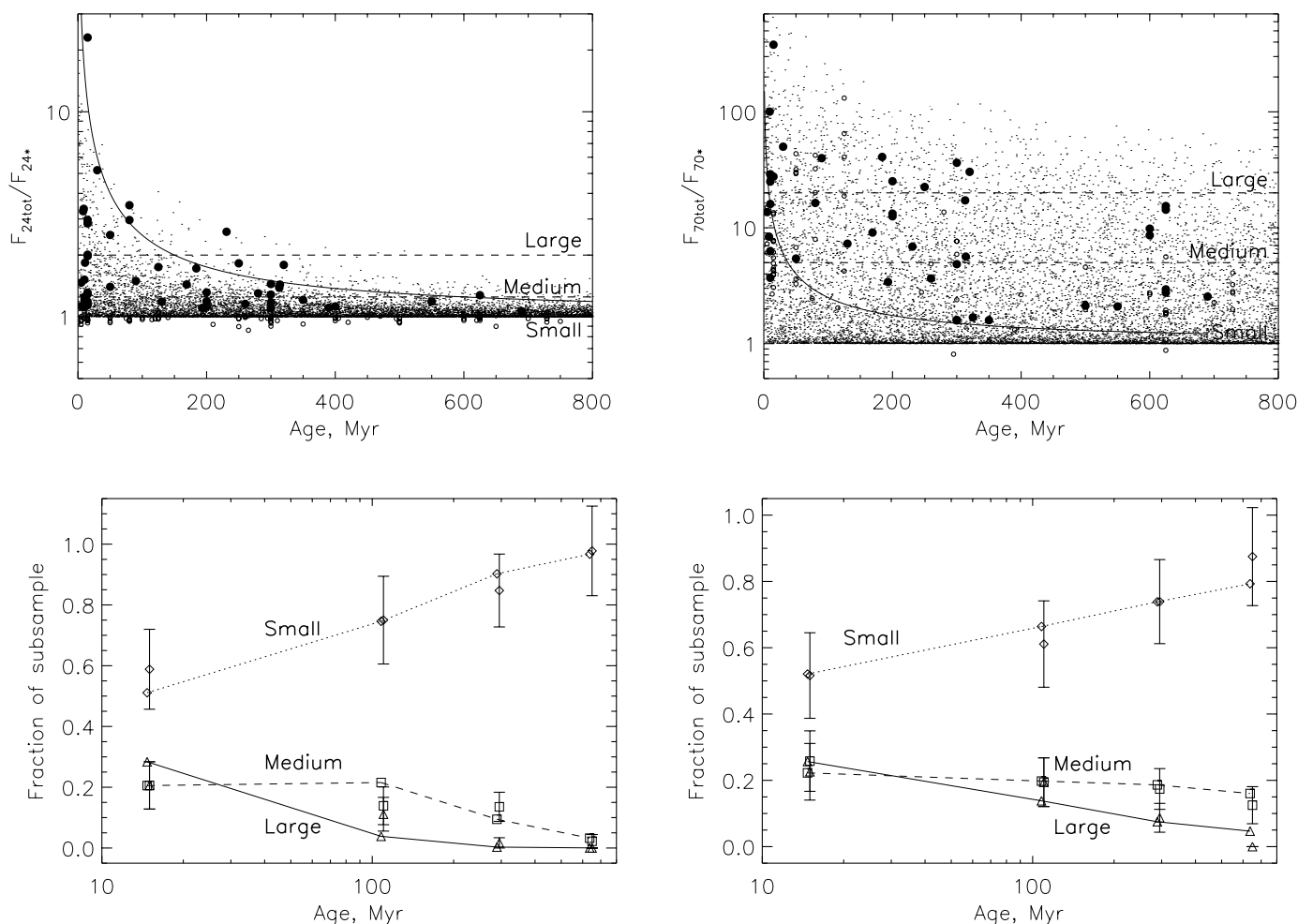
FIG. 2.—Fit of the model population to the distributions of: 24 μm (*left*) and 70 μm (*right*) excesses in Su et al. (2006) (§ 4). The model parameters are unchanged from those of § 3 (Fig. 1), except for a small change in planetesimal strength. *Top*: Total fluxes at 24 and 70 μm flux divided by that of the stellar photosphere (cf. Figs. 4 and 5 of Su et al. 2006). The 10,000 disks in the model population are shown with dots. Stars with excess emission observed at 24 and 70 μm are shown with filled circles in the left and right plots, respectively, while those undetected at 24 μm, or for which upper limits were derived at 70 μm, are shown with open circles. The $150t_{age}^{-1}$ line delineating the upper envelope of the 24 μm detections (Rieke et al. 2005) is shown with a solid line. *Bottom*: Fraction of stars with flux ratios in the different age bins used by Su et al. (2006) for their Fig. 9 (<30 Myr, 30–190 Myr, 190–400 Myr, >400 Myr): $F_{24tot}/F_{24\star} = 1$–1.25 (diamonds = small excess), 1.25–2 (squares = medium excess), >2 (triangles = large excess); and $F_{70tot}/F_{70\star} = 1$–5 (diamonds = small excess), 5–20 (squares = medium excess), >20 (triangles = large excess). Observed values are shown with $\sqrt{N}$ error bars, and model values are joined with dotted, dashed, and solid lines for increasing $F_{tot}/F_{\star}$.

average older than the rest of the population;[2] (3) stars with no apparent excess have limits as low as $f < 10^{-7}$; (4) a large spread of 2 orders of magnitude of fractional luminosity at any given age; (5) older stars have lower fractional luminosity than younger ones; (6) the upper envelope in fractional luminosity falls off $\propto t_{age}^{-1}$, and is not constant as found in Decin et al. (2003); and (7) for disks detected at both 24 and 70 μm, the color temperature distribution is broader at younger ages.

Here we explain these trends by considering the effect of the detection threshold on the subsamples of the model population that are detected at 24 or 70 μm, or at both wavelengths, on three plots of the model population. The model is compared with a sample of 46 A stars for which excess emission was detected at both 24 and 70 μm and so for which the radii of their disks can be estimated; that sample is described in § 4.2.1. The three plots are

the three fundamental disk parameters plotted against each other: f versus r (§ 4.2.2), f versus t_{age} (§ 4.2.3), and r versus t_{age} (§ 4.2.4). A further comparison of the model to the 24 and 70 μm detected sample is given in § 4.2.5.

4.2.1. Sample of 46 A Star Disks Detected at 24 and 70 μm

In the absence of large numbers of resolved images of disks from which to get a direct measure of their radii, the only way to estimate this important parameter is from interpretation of the spectrum of the excess emission, which must be detected at more than one wavelength to allow an estimate, rather than a limit, to be determined. Here we construct a sample of A star disks for which radius estimates can be made since they were all detected at both 24 and 70 μm.

The sample of 46 stars is given in Table 1 and includes:

1. The 35 group I sources in Table 3 of Su et al. (2006) that have excesses detected at both 24 and 70 μm (i.e., excluding HD 23862, for which there is evidence of gas emission lines in its mid-IR spectrum taken with *Spitzer* IRS). The fractional luminosities of these sources were taken from Table 3 of Su et al.

---

[2] HD 188228 in Su et al.'s group II has an age of ~10 Myr and is an exception to the rule they state that young stars with 70 μm excesses also have an excess at 24 μm. However, the remaining seven stars in their group II have ages >325 Myr, and the mean age of their group II stars, ~490 Myr, is significantly older than the rest of the population.
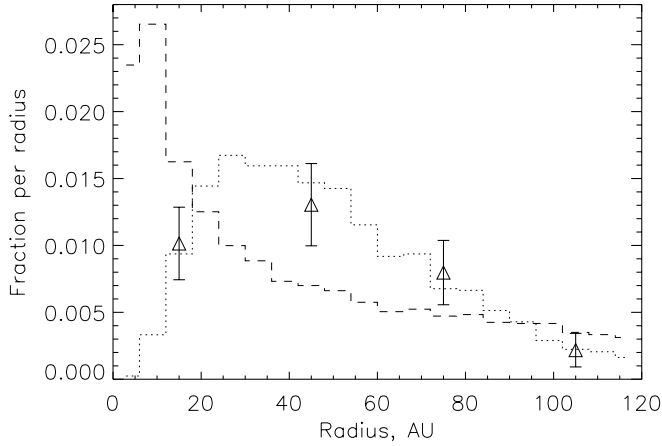
Fig. 3.—Distribution of planetesimal belt radii. That of the whole model population described in § 4 (and shown in Fig. 2) is shown with a dashed line, while that of the subsample of the model population predicted to be detectable at 24 and 70 μm is shown with a dotted line. The observed distribution of radii for the 46 A star disks that have been detected at both 24 and 70 μm (§ 4.2.1) is shown with triangles and $\sqrt{N}$ error bars. The y-axis is the fraction of disks in each sample that fall in the different radius bins (of width 6 or 30 AU).

(2006), and the 24–70 μm color temperature combined with knowledge of the stellar luminosity to infer a planetesimal belt radius from equation (7), i.e., by assuming this arises from blackbody emission. Stellar ages, distances, and spectral types are from Table 1 in Su et al. (2006), and stellar temperatures and masses were estimated from spectral type.

2. Eleven additional stars from the literature for which excess emission has been detected at both 25 and 60 μm by *IRAS*. *Spitzer* observations at 24 and 70 μm for seven of these are available either in the literature or in the archive, and the available observations for these sources were analyzed in the same way as the Su et al. (2006) sources to derive stellar luminosity, dust luminosity, and dust temperature (and so planetesimal belt radius). For the remaining four sources, their 25 and 60 μm fluxes were taken from *IRAS* SCANPI,[3] and these fluxes were analyzed using a process analogous to that used in Su et al. (2006). In that process, spectral types were taken from SIMBAD and used to determine stellar temperatures and masses, and distances were taken from *Hipparcos*. Stellar luminosities were determined by integrating under the spectrum of a Kurucz model atmosphere fitted to the *K*-band flux from 2MASS. The stellar spectrum was also used to estimate the photospheric contribution to the 25 and 60 μm *IRAS* fluxes (having taken the appropriate color correction into account) and so to determine the temperature, radius, and fractional luminosity of the excess emission. Fractional luminosities and radii are consistent for the three sources that overlap with Rhee et al. (2007), who performed similar calculations. The ages of these 11 sources were taken from the literature (HD 1438 from Wyatt et al. 2003a; HD 3003 from Song et al. 2001; HD 9672, HD 21997, HD 110058, HD 158352, HD 172555, and HD 176638 from Rhee et al. 2007; HD 109573 from Stauffer et al. 1995; HD 141569 from Weinberger et al. 2000; and HD 153053 from Chen et al. 2006).

For consistency we checked that the parameters given in Table 1 can be used to predict the observed stellar and excess fluxes using the equations given in this paper. The stellar flux should be given by equation (8), while the excess flux can be de-

rived by rearranging equations (4), (6), and (7) to get the disk flux in Jy at a wavelength λ to be

$$F_{\nu\mathrm{disk}} = 2.95 \times 10^{-10} f r^2 d^{-2} B_\nu\left(\lambda,\ 278.3 L_\star^{0.25} r^{-0.5}\right). \quad (18)$$

Equation (18) predicts the observed disk fluxes at 24 and 70 μm to within 2%, which is to be expected, since these fluxes were used to derive the disk parameters.[4] At wavelengths other than 24 and 70 μm, there may be inaccuracies due to the assumption that the emission spectrum is described by that of a blackbody at a single temperature (e.g., see § 5). The resulting stellar fluxes are also in general agreement, although they are for some stars in error by a factor of up to 2. We attribute this to the shape of the stellar spectrum, which means that a bolometric luminosity cannot be rigidly applied to derive stellar fluxes to a greater accuracy, but consider that this accuracy is sufficient to perform a simple analysis of this sample.

Since some of these disks have been resolved in ground- and space-based imaging, it is worth comparing the resolved sizes with those predicted by this crude analysis of the 24 and 70 μm fluxes. For the disks seen to be confined to rings it is clear that the prediction given in Table 1 underestimates the true size by a factor of 2–3: Fomalhaut is predicted to have dust at 67 AU whereas 133 AU is its observed radius (Kalas et al. 2005), and HR 4796 is predicted to have dust at 27 AU whereas 70 AU is observed (Telesco et al. 2000). Likewise, HD 181327 is reported to have an observed size that is 3 times larger than that predicted using blackbody grains (Schneider et al. 2006). This discrepancy can be readily explained by the fact that the smallest dust grains in their distributions, which dominate the cross-sectional area, emit at a higher temperature than blackbody for a given distance from the star (Wyatt et al. 1999; Wyatt & Dent 2002). For the two young systems HD 39060 (β Pictoris) and HD 141569, the dust is observed to span a large range of radii: from tens of AU out to thousands of AU for β Pictoris with a density distribution that peaks at 75 AU (Kalas & Jewitt 1995; Telesco et al. 2005), and from ~10 to 1200 AU for HD 141569 (Fisher et al. 2000; Clampin et al. 2003). These extended distributions certainly complicate the interpretation of these systems in terms of rings, although it is believed that radiation forces cause the distributions of dust in these systems to extend far beyond those of the planetesimal belts that created them (Augereau et al. 2001), so that the predicted planetesimal belt radii of 24 AU for β Pictoris and 35 AU for HD 141569 are not as inaccurate as they first appear. For Vega, the predicted size of 114 AU is close to the size observed in the submillimeter (Holland et al. 1998), even if the far-IR emission on which the size estimate is based extends out to much larger distances (Su et al. 2005). We have opted to retain the radius derived from the SED modeling for plotting purposes, since these are then derived in a more consistent manner across the data set.

All but four of the disks in this sample were detected by *Spitzer* at both 24 and 70 μm. The remaining four disks have yet to be observed by *Spitzer*, but were detected by *IRAS* at both 25 and 60 μm. Thus, we consider that the sample derived here is representative of those disks which it is possible to detect at 24 and 70 μm, and in the following sections we compare this sample with the subsample of the model population that would have been detected in the study of Su et al. (2006), assuming the detection limits quoted by those authors. The limiting factor for

---

[3] See http://scanpi.ipac.caltech.edu:9000.

[4] The observed disk flux here is the total observed flux less the photospheric contribution. As such there is an uncertainty in the true level of disk flux due to observational uncertainties and the accuracy of the photospheric subtraction.
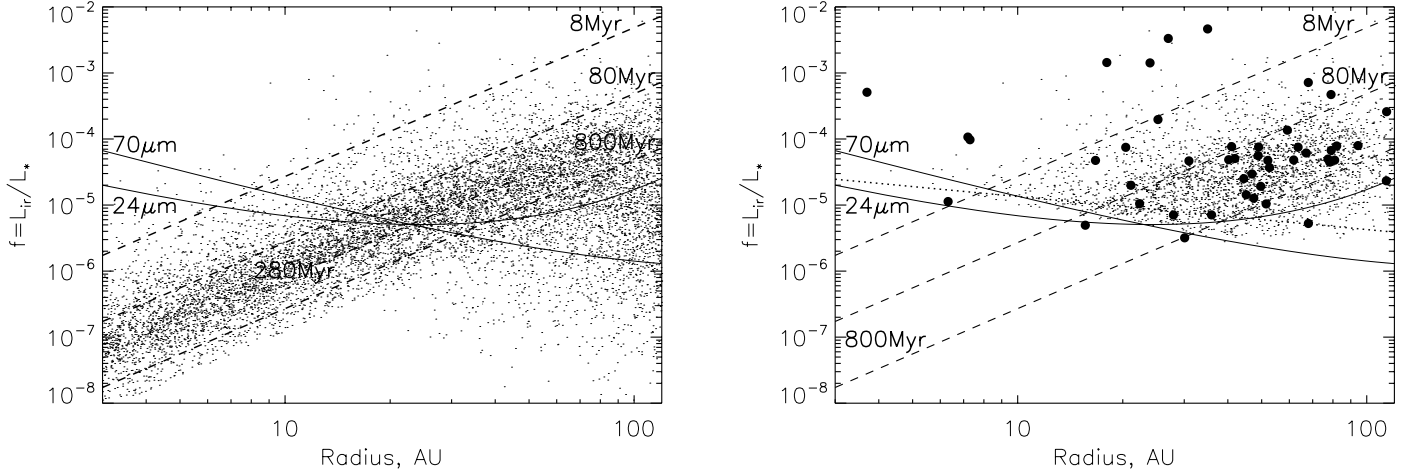
FIG. 4.—Fractional luminosity versus radius. *Left*: The 10,000 disks in the A star population model of Fig. 2 are shown with dots. The detection thresholds of the Su et al. (2006) *Spitzer* observations at 24 and 70 μm ($F_{24\mathrm{disk}}/F_{24\star} > 0.1$ and $F_{70\mathrm{disk}}/F_{70\star} > 0.55$) are shown with solid lines for A0 V stars (eq. [19]). The maximum luminosities for planetesimal belts around A0 V stars of age 8, 80, 280, and 800 Myr in the model are shown with dashed lines (eq. [20]). *Right*: Same as left, except that only disks in the model population that could be detected at 24 and 70 μm are plotted. Also shown with filled circles are the properties of the 46 disks that were detected at both 24 and 70 μm (§ 4.2.1). The dotted line shows the limit below which PR drag becomes important for A0 V stars (eq. [21]).

these observations was not instrumental sensitivity; rather it was the ability to distinguish between photospheric and excess emission. It was thus the accuracy of the extrapolation of the photospheric flux from near-IR to longer wavelengths that determined the detection threshold. A detection required a disk flux relative to the stellar flux at 24 and 70 μm of $F_{24\mathrm{disk}}/F_{24\star} > R_{24\mathrm{det}} = 0.1$ (for a 5 σ detection) and $F_{70\mathrm{disk}}/F_{70\star} > R_{70\mathrm{det}} = 0.55$ (for a 3 σ detection), respectively. Rearranging equations (8) and (18) shows that such detection limits correspond to disks with a fractional luminosity of

$$f_{\mathrm{det}} = 6.0 \times 10^9 R_{\mathrm{det}} r^{-2} L_\star T_\star^{-4} B_\nu(\lambda, \ T_\star)/B_\nu\big(\lambda, \ 278.3 L_\star^{0.25} r^{-0.5}\big).$$

(19)

4.2.2. *Fractional Luminosity versus Radius*

The most valuable plot for interpreting the statistics of debris disk surveys that have detection thresholds given by equation (19) is the plot of fractional luminosity against radius, Figure 4. The 10,000 disks in the model population are shown in Figure 4 (*left*). There is a general trend evident in the upper envelope of the model population following $f \propto r^{7/3}$. This trend can be understood from equation (14), and considering that when $X_c \ll 1$, then $G(11/6, \ X_c) \propto r^{-5/6}$, and so $f_{\mathrm{max}} \propto r^{7/3}$ (Wyatt et al. 2007). Lines showing the maximum possible luminosity for planetesimal belts in the model that have ages of 8, 80, and 800 Myr, assuming these are around A0 V stars with the parameters for $Q_D^\star$, e, and D_c, described in § 4.1, are also shown on this figure. These lines are approximately

$$f_{\mathrm{max}} \approx 1.2 \times 10^{-6} r^{7/3} t_{\mathrm{age}}^{-1}.$$

(20)

In other words, the maximum possible luminosity for planetesimal belts of a given radius depends only on age, and the upper envelope in the model population is thus determined by the youngest age of its disks.

The lines of maximum luminosity are extremely useful, since the evolution on Figure 4 of any one planetesimal belt in the model, with initial parameters of radius r_1 and fractional luminosity f_1, is for it to remain stationary at (r_1, f_1) while its age is $t_{\mathrm{age}} < 1.2 \times 10^{-6} r^{7/3} f_1^{-1}$ Myr, and then for its fractional lumi-

nosity to decrease at later times such that it is always found at (r_1, f_{max}) at an age $t_{\mathrm{age}} > 1.2 \times 10^{-6} r^{7/3} f_1^{-1}$ Myr. This means that a disk of a given age either lies on the appropriate line of maximum luminosity or below it, so that, e.g., the subsample of model disks that are older than 80 Myr are (some fraction of) the disks that lie below the line of maximum luminosity for 80 Myr. Note that while this is useful for illustrating the trends in the data it should not be applied too rigidly, since these lines are also a function of spectral type, and their exact location depends on parameters like $Q_D^\star$, e, and D_c, which may vary among disks.

Also shown in Figure 4 (*left*) is the detection limit at 24 and 70 μm appropriate for planetesimal belts around A0 V stars, assuming the detection thresholds given in § 4.2.1 (eq. [19]). The detection threshold at 24 μm is roughly flat at $f_{24\mathrm{det}} = (0.5\text{–}2) \times 10^{-5}$ across all radii, while that at 70 μm falls more than an order of magnitude across the range 3–120 AU. Disks in the model population that we predict could be detected at 24 and 70 μm would lie above both of these lines (noting, however, that the location of the line is also spectral-type dependent). Such a subsample is shown in Figure 4 (*right*), where the sample of observed disks that were actually detected at 24 and 70 μm (§ 4.2.1) is also plotted. To a large degree, the observed population is well described by the model population, both in terms of the lower envelope (described by the 24 and 70 μm detection limits), and the upper envelope (described by a $\propto r^{7/3}$ power law and close to the line of maximum luminosity for disks a few Myr old), as well as the distribution of disks in between, which is more dense between the lines of maximum luminosity for 80 and 800 Myr. A fit to the population of observed disks gives $f \propto r^{-0.1 \pm 0.3}$ with a large spread at each radius, which is not inconsistent with that expected from the model population for disks detected at 24 and 70 μm ($f \propto r^{0.6}$). The agreement is closer (fit to observed population of $f \propto r^{0.9 \pm 0.3}$) when the systems mentioned in the following paragraph are removed.

Closer inspection shows that the disks that lie above the 8 Myr maximum luminosity line for disks around A0 V stars are the disks with well known ages in the range 5–12 Myr (HD 39060, HD 109573, HD 110058, HD 141569, and HD 172555) and three stars that have f/f_{max} in the range 30–100, and so appear unusually bright for their age (HD 3003 at 50 Myr, HD 38678 at 230 Myr, and HD 115892 at 350 Myr; Table 1). The
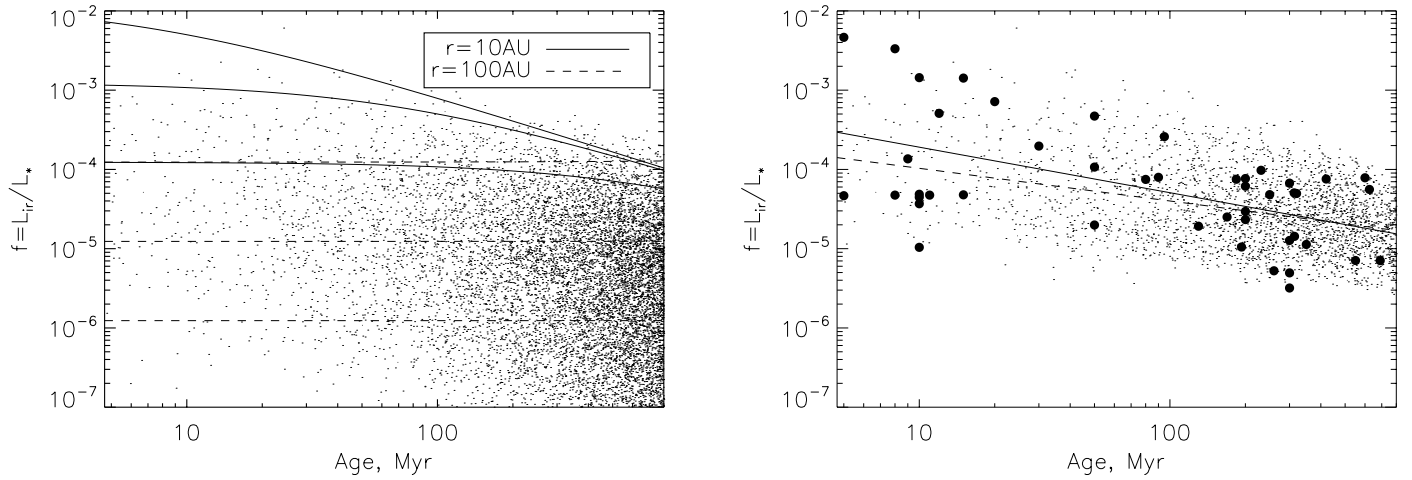
Fig. 5.—Fractional luminosity versus age. *Left*: The 10,000 disks in the A star population model of Fig. 2 are shown with dots. The evolutionary tracks of individual planetesimal belts at 10 and 100 AU around A0 V stars are shown with solid and dashed lines, respectively, for starting disk masses of 1, 10, and 100 $M_\oplus$ (with higher masses corresponding to higher fractional luminosities at young ages). *Right*: Same as left, except that only disks in the model population that could be detected at 24 and 70 μm are plotted. Also shown with filled circles are the properties of the 46 disks that were detected at both 24 and 70 μm (§ 4.2.1). The solid and dashed lines show fits to the observed and model disk populations, respectively.

presence of the disks of 5–12 Myr stars above the 8 Myr line is to be expected, since the planetesimal belts in these systems either must be, or are likely to be <8 Myr old. Even if the star itself is older than 8 Myr, we still need to allow some time for the planetesimal belt to form, and if this occurs on the same time-scale that it takes for protoplanetary disks to dissipate, then it takes ~6 Myr (Haisch et al. 2001). Also, at such a young age, there is the possibility that these systems have yet to reach equilibrium, and that this early phase is characterized by an unusually high quantity of small dust grains. Whether the three unusually bright stars are in a transient phase (Wyatt et al. 2007), or have unusual planetesimal belt properties remains to be seen.

Understanding how the detection limits (eq. [19]) and constraints from the maximum possible luminosity for a given age (eq. [20]) appear on the plot of fractional luminosity against radius (Fig. 4, *left*) readily explains trends (1)–(3) given in § 4.2 (Su et al. 2006): (1) the model predicts that disks that are detected at 70 μm but not 24 μm should lie in the region below the 24 μm threshold and above the 70 μm threshold on this plot, with f in the range 10^{-6} to 3×10^{-5} (for A0 V stars), depending on their radius. In contrast, those detected at both wavelengths, which should lie above both thresholds, would have f in the range 5×10^{-6} to 10^{-2} (for A0 V stars). Thus, the model predicts that the range in f should be systematically higher for disks detected at both wavelengths than for those detected only at 70 μm, as found by Su et al. (2006). (2) The region of parameter space occupied by disks that are detected at 70 μm but not at 24 μm also lies entirely below the line of maximum luminosity for 280 Myr (for A0 V stars; Fig. 4). This means that the only disks in this region of parameter space that are younger than 280 Myr must be those of initially low mass for which the most massive objects within them have yet to come to collisional equilibrium. This means that this population has a higher average age (460 Myr) than the rest of the population (400 Myr). This is consistent with the findings of Su et al., since the mean age of their group II sources (i.e., those detected at 70 but not 24 μm) is higher than average at ~490 Myr. The model can also be used to analyze the population of disks that are expected to be detected at 24 but not 70 μm (i.e., Su et al. 2006 group V sources). In the model, such disks have small radii (<23 AU for A0 V stars) and lie above the 280 Myr line of maximum luminosity (for A0 V

stars), meaning that there can be no disks in this population that are older than this limit, and that the mean age of this population is ~150 Myr. Indeed, the oldest star in Su et al. (2006) group V is 400 Myr old, and the mean age of their group V sample is 100 Myr.[5] (3) The lowest excess in the model population is $f \approx 10^{-9}$, and 28% of stars in this population have excesses lower than 10^{-7}, in agreement with nondetections at this level in Su et al. (2006).

4.2.3. *Fractional Luminosity versus Age*

The fractional luminosity of the 10,000 disks in the model population are shown in Figure 5 (*left*) as a function of stellar age. Also shown on this plot are lines showing the evolution that a planetesimal belt at 10 and 100 AU would take assuming starting masses of 1, 10, and 100 $M_\oplus$. As described in § 2.1, this evolution remains flat until the largest planetesimals collide, at which point the fractional luminosity falls off $\propto t_{\rm age}^{-1}$. For the planetesimal belt at 100 AU, the largest planetesimals do not have a chance to reach collisional equilibrium over the assumed 800 Myr main-sequence lifetime of the star, while for the planetesimal belt at 10 AU, this equilibrium is reached in the range a few Myr to a few hundred Myr, depending on starting mass. The upper envelope in the model population can be described as being reasonably flat at $f \approx 10^{-3}$ until an age of ~100 Myr, at which point it falls off. The falloff rate is slightly flatter than $\propto t_{\rm age}^{-1}$, which is because the brightest disks at any given age are at different radii for different ages. For example, the upper envelope for ages <100 Myr is reasonably well characterized by the evolution of the 100 $M_\oplus$ planetesimal belt at 10 AU shown on Figure 5 (*left*), whereas the evolution of the 100 $M_\oplus$ planetesimal belt at 100 AU has a higher luminosity than that at 10 AU at ages >600 Myr.

The subsample of the model population that can be detected at 24 and 70 μm is shown in Figure 5 (*right*) and exhibits the same upper envelope. The lower envelope of this population

---

[5] Some of the Su et al. group V sources were not observed down to the limit $R_{\rm 70det} = 0.55$, e.g., due to cirrus confusion. Thus, more sensitive observations may find 70 μm excesses at $R_{\rm 70det} > 0.55$ in this sample. However, this would not affect the conclusion that bona fide group V sources are, on average, younger than the rest of the population.

also falls off slowly with time, not because the detection limit drops, but because a smaller fraction of the stars at younger ages have luminosities approaching that limit, whereas collisional processing has reduced the fractional luminosities of older stars so that many are pushed below the detection threshold (particularly for disks at small radii). The model thus explains trends (4) and (5) of § 4.2 (Su et al. 2006). (4) The spread in fractional luminosity at any given age is around 2 orders of magnitude in both the observed and model populations. (5) Both the model and observed populations have lower fractional luminosities for disks around older stars than around younger ones, with the model population exhibiting a $f \propto t_{age}^{-0.39}$ falloff that is in excellent agreement with the observed population for which $f \propto t_{age}^{-0.57\pm0.13}$ (compared with $f \propto t_{age}^{-0.6}$ quoted in Su et al. [2006] for their observations).

The biggest difference between the model and observed populations is that the model assumes that stellar ages are uniformly distributed between 0 and 800 Myr, which means that the model predicts that 30% of the population detected at 24 and 70 μm should be older than 400 Myr, whereas just 11% of the observed population are that old. The most likely cause for this discrepancy is the fact that the mean age of the stars searched for 24 and 70 μm excesses is younger than the 400 Myr mean age of the model population. The mean age of the Su et al. (2006) sample is 270 Myr, which may be attributable to a bias in the way the sample was chosen, or to the fact that A0 V stars reach the end of the main sequence at $\sim$400 Myr, which means that a dearth of >400 Myr early-type stars is to be expected in any sample of main-sequence stars (Greaves & Wyatt 2003). The fact that the model provides a close fit to the fraction of stars from any given age range that lie in specific ranges of fractional excess flux (§§ 3.2 and 4.1) means that the age distribution of the observed sample is immaterial, suggesting that a sudden disappearance of disks at $\sim$400 Myr (Habing et al. 1999) is not required to explain the statistics. However, given that 39 stars in Su et al. (2006) were observed in the >400 Myr population, and that the model predicts that 46% (i.e., 18) of these should have disks above the nominal 70 μm detection threshold quoted in that paper, then the observed number of detected disks (3) is only consistent with the model when one takes into account the fact that not all of the 39 stars were observed down to $R_{70det} = 0.55$, e.g., because of cirrus confusion. Almost all (35) of the 39 were observed to $R_{70det} = 5$, and the model predicts that 17% (i.e., 6) of these should have been detected at this level, which is consistent with the observed number. In other words we predict that, unless there is some mechanism destroying these disks at $\sim$400 Myr, then more disks remain to be detected around the >400 Myr star sample at the nominal 70 μm detection threshold.

The evolution of the upper envelope discussed in trend (4) (§ 4.2; Su et al. 2006) is also in agreement with the model, since we find a falloff in the upper envelope that is close to $\propto t_{age}^{-0.9}$. In answer to the discrepancy with the Decin et al. (2003) result that showed a maximum fractional luminosity that is constant with age, we first note that this applied to disks around stars of all spectral types. When considering their results only for A stars, we find an evolution which is in agreement with that of our observed sample, with the exception of HD 22128, an A5 star for which Decin et al. (2003) quote an age of $\sim$1.4 Gyr and a fractional luminosity of 70×10^{-5} (i.e., which would lie off to the right of our Figure 5, *right*, somewhat above the predicted model population). We thus consider that the anomalous system HD 22128 could have disk properties that make it unusually bright, it could be in a transient state, or its luminosity or age could have been miscalculated. Indeed, an age of 320 Myr has
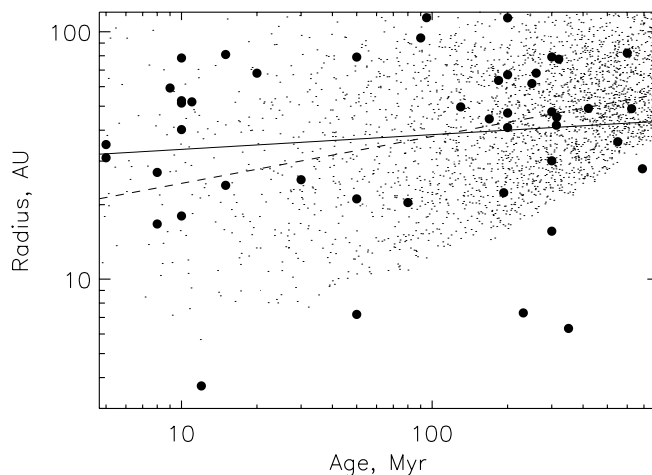

FIG. 6.—Planetesimal belt radius vs. age. The model population of Fig. 2, shown with dots, includes just those disks that could be detected at both 24 and 70 μm. Also shown with filled circles are the properties of the 46 disks that were detected at both 24 and 70 μm (§ 4.2.1). Least-squares fits to this evolution are shown with solid and dashed lines for the observed and model populations, respectively.

also been quoted for HD 22128 (Decin et al. 2003). Further, recent MIPS observations show that the source is extended at 24 and 70 μm on >1000 AU scales. Since such emission is unlikely to originate in a disk, this suggests that the luminosity of the debris disk based on bolometric far-IR observations is an upper limit and the existence of a debris disk in this system is suspect.

4.2.4. Radius versus Age

The radii of the 10,000 disks in the model population are shown in Figure 6 as a function of stellar age. Since in this model the radius does not change with age, we have plotted only those disks in the model for which it is possible to detect at 24 and 70 μm, and compared these with the properties of the observed population. The most noticeable trend of the model population is that at any given age it is only disks that have radii larger than a certain limit that can be detected, and that this limit increases with age. This can be readily understood from Figure 4 (*left*). For example, disks that are both $\sim$80 Myr old and detected at 24 and 70 μm must lie below the 80 Myr line of maximum luminosity on that figure, and above the 24 and 70 μm thresholds. This is a region of parameter space that permits only disks with radii >16 AU (for A0 V stars), and that does not extend down so far in radius at later ages (and encompasses a much smaller area). Physically this is because planetesimal belts at smaller radii process their mass faster and so fall below the detection threshold at younger ages (i.e., it does not mean that planetesimal belts at this radius do not exist). This is manifested as an apparent increase in the radius of planetesimal belts with age, with a least-squares fit to the population of detected disks in the model increasing $\propto t_{age}^{0.20}$, although there is still a large spread in radii at any age. While the effect is small, the increasing size of the empty region with age means that the radius distribution (and so the color temperature distribution) is broader at younger ages, which means that the model also reproduces trend (7) (§ 4.2), seen by Su et al. (2006). The modest apparent increase in size with age is also consistent with the observed population, for which we derive a reasonably flat evolution of $\propto t_{age}^{0.06\pm0.07}$ (although note that a steeper evolution $\propto t_{age}^{0.09\pm0.05}$ would be inferred if the anomalous sources discussed below are removed). A flat distribution of radii with age was also observed in the

submillimeter study of Najita & Williams (2005) which included disks around stars of all spectral types. It was also reported by Rhee et al. (2007), although these authors suggested that the upper envelope in radius may increase across the range 100–1000 Myr, an observation which is not predicted in our model, and only seen with low significance in our observed population.

However, there is a distinct anomaly in that six of the observed disks fall in the region of Figure 6 in which there are no model disks: HD 38678, HD 115892, and HD 172555 lie well within the forbidden region, while HD 2262, HD 3003, and HD 106591 lie close to the upper edge of this region. We offer two possible explanations for these systems. The first is that these are systems which are undergoing a transient period of high dust luminosity (Wyatt et al. 2007). This has already been discussed as a possibility for HD 38678 in § 4.2.2, based on its high luminosity for its age (this was also suggested in Moerchen et al. 2007). The other possibility is that the fitting procedure has underestimated the radius of the planetesimal belt.

In addition to the possibility that a dust temperature that is higher than blackbody has caused the dust location to be underestimated, it is also possible that the dust is located closer to the star than the planetesimal belt because of the action of Poynting-Robertson (PR) drag. PR drag becomes important when $10^4 f(r/dr)(r/M_\star)^{1/2}/\beta < 1$ (Wyatt 2005), where β is the ratio of the radiation force to that of gravity of the star, since this is when the collisional lifetime of the dust is equal to the time it would take to reach the star by the drag force. Assuming, as in the model here, that the dust luminosity is dominated by the smallest dust in the distribution with $\beta = 0.5$, this limit is given by $f < f_{\rm pr}$, where

$$f_{\rm pr} = 50 \times 10^{-6}(dr/r)\sqrt{M_\star/r}, \qquad (21)$$

and this is shown on Figure 4 (right) for A0 V stars assuming $dr/r = 0.5$, and compared with the observed fractional luminosity for the 46 disks in Table 1. The proximity of this PR drag limit to the detection threshold at 24 and 70 μm illustrates how PR drag may become important for disks close to the detection threshold of *Spitzer*, at least for early-type stars.

The details of how the model would be affected by PR drag below (or approaching) this level are not clear without further modeling, but the nature of the drag force means that a lower dust radius (but not planetesimal belt radius) would be expected. Thus this is one possible explanation for the close proximity of dust from the stars HD 2262, HD 106591, and HD 115892, all of which have $f/f_{\rm pr} < 1$. It may be possible to test this observationally, since in the extreme situation where PR drag dominates the dust distribution the surface density of the dust disk would be uniform from the planetesimal belt all the way in to the star, leading to an emission spectrum that increases linearly with wavelength ($F_\nu \propto \lambda$; Wyatt 2005). One other source for which PR drag may be important in shaping the inner edge of its dust disk is HD 19356, for which $f/f_{\rm pr} < 1$, while a further 11 disks have $1 < f/f_{\rm pr} < 5$ (Table 1).

4.2.5. Accuracy of $f_{\max}$

Figure 7 shows the ratio of observed fractional infrared luminosity to the maximum luminosity expected for disks at the inferred radius around stars of the age and spectral type of the hosts; i.e., $f/f_{\max}$. This is found for the sample of 46 stars detected at 24 and 70 μm (§ 4.2.1) to be peaked at $f/f_{\max} \approx 1$, but extending to around a factor of 100 higher and lower; the values for this sample are also given in Table 1. The subsample of the
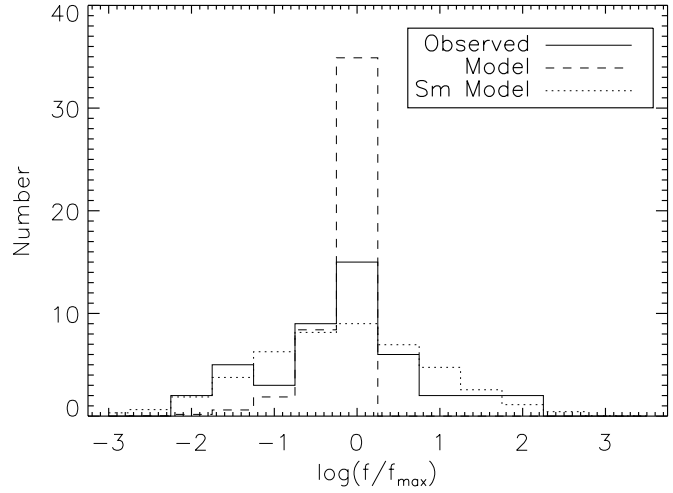

FIG. 7.—Histogram of the infrared luminosity divided by the maximum luminosity possible in the model for a disk of this age, spectral type, and radius (assuming planetesimal belt properties inferred in § 4). The distribution for the observed sample of 46 disks that were detected at both 24 and 70 μm (§ 4.2.1) is shown with a solid line. The distribution for disks in the model population of Fig. 2 that could be detected at 24 and 70 μm scaled to a population of 46 disks is shown with a dashed line. A Gaussian smoothing of 1 dex applied to the model population distribution is shown with a dotted line.

model population detectable at 24 and 70 μm is also shown in this figure, and this peaks much more sharply at $f/f_{\max} \approx 1$, with a tail to lower $f/f_{\max}$. As expected, there are no disks in the model with $f > f_{\max}$, and the fact that the majority of the model disks have $f \approx f_{\max}$ indicates that the majority of the detected disks (in the model) are evolving with their largest planetesimals in collisional equilibrium.

The observed population has a noticeably broader distribution of $f/f_{\max}$ than does the model population. We interpret this as a consequence of the assumption that all disks have the same planetesimal properties. In reality disks would be expected to have a distribution of properties, and the parameters (D_c, $Q_D^\star$, and e) used in the expression for $f_{\max}$ would only be representative of the population as a whole rather than of individual disks. Thus the breadth of the observed distribution may be indicative of the distribution of disk properties. To estimate this breadth we show in the same figure a smoothed model in which the distribution has been smoothed by a Gaussian of width 1 dex, which fits the observed distribution well, and suggests a similar breadth in the distribution of $D_c^{0.5} Q_D^{\star 5/6} e^{-5/3}$ about the mean values given in equation (17). Since the $f/f_{\max}$ distribution will also have been smeared out due to uncertainties in the observed (or inferred) disk properties, notably r and f, the true distribution of $D_c^{0.5} Q_D^{\star 5/6} e^{-5/3}$ is likely to be much smaller than 1 dex. It is, of course, also possible that some of the disks inferred to have $f > f_{\max}$ are in a transient phase (Wyatt et al. 2007), which would suggest an even narrower distribution of $D_c^{0.5} Q_D^{\star 5/6} e^{-5/3}$ for the population of disks that are in steady state. This indicates a large degree of uniformity in the properties of A star disks.

The most likely candidates for transient emission around A stars are readily identified in Table 1 as those with $f/f_{\max} > 10$: HD 3003, HD 38678, HD 115892, and HD 172555. However, since none of these reaches the threshold $f/f_{\max} > 100$, we do not claim that any of these must be transient, but point out that their properties would have to be extreme compared with the rest of the A star population for their dust emission to be explained by steady state collisional processing of planetesimal

belts.[6] The inferred breadth of the distribution indicates that a disk with $f/f_{max} > 100$ is a 2 σ deviation, while $f/f_{max} > 1000$ is a 3 σ deviation. We also note that the blackbody assumption would tend to overestimate the value of f/f_{max}, since underestimating the radius by a factor of 3 would lead to an overestimation of f_{max} by a factor of 13 and so reduce the factor f/f_{max} by an order of magnitude. In other words, it is not possible to conclude that the disks with $f/f_{max} = 10$–100 represent a significant deviation from the disks found around the remainder of the A star population.

5. PREDICTIONS FOR SCUBA-2 LEGACY SURVEY

While the fact that the model population can explain the available far-IR statistics with steady state collisional evolution is important, this model population can also be used to make predictions for what we can expect to find in future debris disk surveys. Since the model was originally constrained by a fit to the 24 μm statistics, in essence the first of those predictions was for the far-IR surveys at wavelengths other than 24 μm, which § 4 showed to be confirmed. This section demonstrates the further applicability of the model by making predictions for the outcome of the SCUBA-2 legacy debris disk survey. This is an unbiased 850 μm survey of the nearest 100 stars in each of the spectral types A–M (i.e., 500 stars in total; Matthews et al. 2007), and will be sensitivity limited down to the confusion limit which gives a 3 σ limit of $F_{850lim} = 0.002$ Jy. For A stars the survey extends out to around 45 pc.

The model is able to make predictions for the 850 μm flux of the A star population through application of equation (18) to get the disk flux, as well as using equation (8) to get the stellar flux (although this generally falls below the detection threshold). Comparing the flux predicted by equation (18) with that of the seven A stars in the literature with measured 850 μm fluxes (HD 109573, Greaves et al. 2000; HD 39060, HD 216956, and HD 172167, Holland et al. 1998; HD 141569, Sheret et al. 2004; HD 21997 and HD 14055, Williams & Andrews 2006) shows that this equation overestimates the disk flux by an amount X_{850}, where X_{850} for this population lies in the range 2–8, with a median value of 4.0. This is to be expected, since it is known that the emission spectrum falls off steeper than a blackbody at wavelengths beyond ~70 μm (e.g., Dent et al. 2000) because of the low emission efficiency of the small dust grains which dominate the cross-sectional area in the disk. The factor X_{850} is expected to depend on a combination of the dust size distribution, compositional properties, planetesimal belt radius, and stellar spectral type. Thus, when deriving 850 μm fluxes for the model population we reduced the flux found from equation (18) by a factor of $X_{850} = 4$. The ability to estimate submillimeter flux with reasonable accuracy from extrapolation of far-IR data is in agreement with the conclusion of Rhee et al. (2007), who found a strong correlation of dust masses derived from submillimeter fluxes, $M_{850} = F_\nu d^2[\kappa_\nu B_\nu(\lambda, T)]^{-1}$, with f derived from far-IR fluxes. Indeed, our model reproduces the trend shown in their Figure 5, since with a dust opacity of 0.17 m^2 kg^{-1} and a factor of $X_{850} = 4$ our model predicts $f/M_{850} = 14r^{-2}$ (in units of $M_\oplus^{-1}$), exactly as observed by Rhee et al. (2007) for A stars.

Figure 8 shows the predictions of the model for the fractional luminosity versus radius of the subsample of the model population that have 850 μm fluxes above the detection threshold of
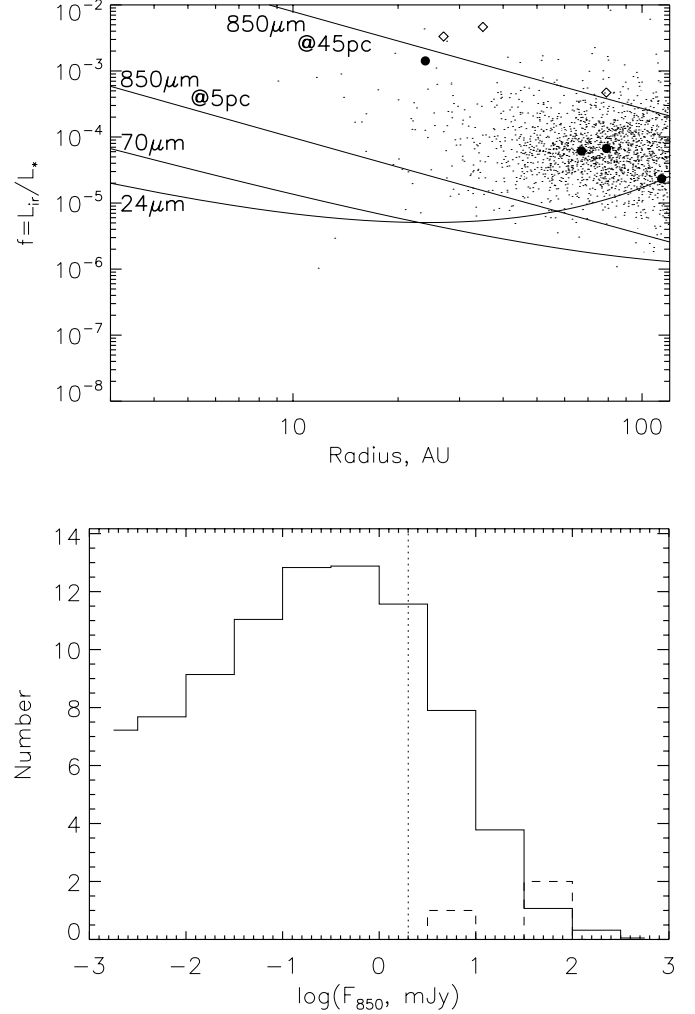

FIG. 8.—Predictions of the model population of Fig. 2 for the outcome of the SCUBA-2 legacy survey, an unbiased survey at 850 μm of the nearest 100 A stars. *Top*: Fractional luminosity of the subsample of the model population which is both within the survey limits (<45 pc), and which has a predicted flux above the sensitivity limit of the SCUBA-2 survey ($F_{850disk} > 2$ mJy; *dots*). The solid lines are the detection thresholds of 24 and 70 μm *Spitzer* observations of Su et al. (2006), and the 850 μm detection threshold for disks at 5 and 45 pc in the survey; all of these detection thresholds apply to disks around A0 V stars. The disks of A stars at <45 pc that have already been detected at 850 μm are shown with filled circles, while those that have been detected but lie beyond 45 pc are shown with diamonds. *Bottom*: Histogram of the distribution of 850 μm flux expected for the 100 A stars within 45 pc. The detection limit is shown with a dotted line. The dashed line shows the stars in the survey already detected at 850 μm.

2 mJy (noting that all of these are also within the survey threshold of 45 pc). Also shown are the seven A star disks with submillimeter detections, indicating the four of these that are within 45 pc. All but one of the four within 45 pc will appear in the SCUBA-2 survey; HD 39060 is excluded, since it is below the declination limit of −40°. There is good agreement between the model and observed populations inside 45 pc, insofar as it is possible to say with such small number statistics. Since the submillimeter detection limit is determined by the instrumental sensitivity, rather than by the accuracy of the photospheric calibration, it is no longer described by equation (19), but can be given by

$$f_{det} = 4.3 \times 10^{10} X_{850} F_{850lim} (d/r)^2 / B_\nu(\lambda, 278.3 L_\star^{0.25} r^{-0.5}),$$

(22)

---

[6] Note that a size of 3 AU for HD 38678 as inferred from mid-IR imaging (Moerchen et al. 2007) would reduce its maximum possible fractional luminosity given its age, f_{max}, by a factor of 7, and so would support the transient nature of this source.

and so is distance dependent. This limit falls with planetesimal belt radius, because for disks at a given distance it is easier to detect those of lower fractional luminosity if they are at larger distance from the star, since their lower temperature at larger distances is more than compensated by the larger cross-sectional area of material. The SCUBA-2 detection limit is plotted on Figure 8 for A0 V stars at 5 and 45 pc, assuming their disks have $X_{850} = 4$. The lower envelope of the model population is thus naturally explained by the small number of A stars that are close to us (of order 14 of the 10,000 are within 5 pc). It is tempting to suggest that the lower envelope of the detected disks is explained in the same way, although with just four disks the lower envelope is not so meaningful. In any case, it is the nearest disks which are detectable in the submillimeter, while for those in a given distance range it is predominantly large disks, or those closer in with high fractional luminosity, that can be detected.

Figure 8 (*bottom*) shows the histogram of the 850 μm fluxes of the model population (noting that this population should be representative of the SCUBA-2 survey sources, since all are within 45 pc). The model predicts that 17 of the 100 stars in the SCUBA-2 A star sample should have a flux above the detection threshold of 2 mJy. Of those 17 five would be expected above 10 mJy and eight in the range 3–10 mJy, with the remaining four detected with 3–4.5 σ confidence at 2–3 mJy. The histogram also shows the submillimeter flux distribution for the three A stars already detected, showing that we already know of two stars within 45 pc with fluxes above 10 mJy (HD 172167, HD 216956), while we know of just one in the range 3–10 mJy (HD 14055). Thus the SCUBA-2 survey is expected to discover three new bright disks >10 mJy, but can expect to find a further seven new disks at 3–10 mJy levels. The >10 mJy sources are particularly interesting, since at such a level of flux it is possible to resolve the structure of the disks (Holland et al. 1998; Wyatt et al. 2005), and indeed the model predicts that 60% of these will have an angular size of >6″ (noting that all may be larger than this given that the blackbody assumption underestimates the true disk size by a factor of up to 3; Schneider et al. 2006). It is also possible to extract some information on the spatial distribution of the 3–10 mJy sources, e.g., giving a direct measure of the size and inclination of the disk (Greaves et al. 2004), with around 23% of these predicted to be larger than 6″.

It may even be possible to extract information from the 83 stars without detected disks, since they are predicted to have a mean flux of 0.60 mJy, of which 0.26 mJy is the mean disk flux and 0.34 mJy is the mean stellar flux. By co-adding their data, the statistical noise level would be reduced to $0.7/\sqrt{83} = 0.077$ mJy, suggesting that it should be possible to get a positive detection of the photospheric emission, and also to discern whether there is an excess coming from the disks with $\sim 3 \sigma$ confidence. However, contamination from extragalactic sources that lie within the SCUBA-2 beam would have a signal of comparable magnitude to the mean disk flux and would reduce our ability to make a conclusive detection of disk emission from this population.

The model predicts that there will be little age dependence within the sample of disks detected by SCUBA-2, in agreement with the result of Rhee et al. (2007), who estimated the mass evolution based on far-IR observations. For example, the model predicts that the mean age of the detected sample is ~ 340 Myr (compared with 400 Myr for the whole population), with a roughly even number of disks (8–9) detected in both the <300 Myr and >300 Myr age bins, which will be indistinguishable from that expected if there were no age dependence (six in the <300 Myr and 11 in the >300 Myr samples). Naturally, SCUBA-2 is in-

clined to detect disks with low values of X_{850}, i.e., those for which their emission is more like blackbody (which would be inferred to be composed of large grains). However, given the small range observed in X_{850}, this dependence is very slight and would affect mainly those disks detected close to the sensitivity threshold. There is also predicted to be a small spectral type dependence, in that 19% of stars later than A3 V are predicted to be detected by SCUBA-2, compared with 15% of those earlier than A3 V. This arises because, while disks of lower fractional luminosity can be detected around earlier type stars, $f_{det} \propto L_{\star}^{-0.25}$ (eq. [22]), the fractional luminosities of their dust belts are also much lower because of the higher dust blow-out radius, $f_{max} \propto L_{\star}^{-0.5}$ (eq. [14]). We do not anticipate that this would be detectable within the A star sample; however, it suggests that the detectability of Sunlike stars could be high, should their disk population be described by the same parameters as for the A stars.

Figure 8 (*top*) also shows the 24 and 70 μm detection limits of the *Spitzer* survey of Su et al. (2006). This shows that almost without exception (99.9%) the disks that can be detected by SCUBA-2 at 850 μm are also detectable by *Spitzer* observations at 70 μm with a detection threshold of $R_{70det} > 0.55$, while most (61%) of those detectable by SCUBA-2 are also detectable by *Spitzer* at 24 μm. In other words, 10 of the 100 A stars in the SCUBA-2 sample should be detectable at 24, 70, and 850 μm, while seven should be detectable at 70 and 850 μm, but not at 24 μm; the combination of submillimeter and far-IR data would be very important for constraining the dust temperature in these disks. While this suggests that the survey could equally well be done at 70 μm, there are three important points to consider. (1) First, not all of the sample has been observed with *Spitzer*—the Su et al. (2006) sample includes 42 sources within 45 pc (of which 20 were detected at 70 μm), which assuming even coverage across the sky means that 34 of these should fall in the SCUBA-2 survey (which has declination limits of $-40°$ and $+80°$). This implies that 2/3 of the SCUBA-2 A star sources have not previously been searched for disks in the far-IR (although bright disks may have turned up in *IRAS* surveys which have a detection threshold well above that shown in Fig. 8). It is also not possible to scrutinize all stars with *Spitzer* to the level of $R_{70det} = 0.55$ due to cirrus confusion. Thus, it is predicted that the SCUBA-2 survey will turn up a significant number of genuinely new discoveries. (2) Second, it is important to emphasize the unbiased nature of the SCUBA-2 survey. Several sources have recently been identified as possessing excess emission in the submillimeter even when no excess is present in far-IR surveys (Wyatt et al. 2003a; Holmes et al. 2003; Najita & Williams 2005). These disks must be cool (<40 K) and at large radius; e.g., extrapolation of the detection thresholds in Figure 8 to larger radii indicates that the submillimeter is more sensitive than 70 μm surveys to disks that are >210 AU at 5 pc for A0 V stars and >74 AU at 5 pc for A9 V stars. Since the model population was constrained by 24 and 70 μm surveys, there was no need to invoke a population of disks of large radius, although we know that dust exists around young A stars to hundreds of AU (Kalas & Jewitt 1995; Clampin et al. 2003). Thus the predicted detection statistics should be viewed as a lower limit, with many large disks being detected at 850 μm which cannot be detected in the far-IR. Previous unbiased submillimeter surveys suggest that $\sim 15\%$ of stars could have disks too cold to detect in the far-IR, which could push the detection rate to $\sim 30\%$ for the SCUBA-2 A star survey. (3) Even discounting the ultracool disks discussed in (2), the submillimeter statistics will set important constraints on the distribution of the planetesimal belt radii, since the predictions made here are very sensitive to that

distribution. For example, with a radius distribution $N(r) \propto r^{-0.5}$, which is not ruled out in the present study at the 1 σ confidence level, the model would predict that 22 of the 100 A stars would be detected at >2 mJy, of which seven would be >10 mJy.

6. CONCLUSIONS

A simple model for the steady state evolution of dust luminosity for planetesimal belts evolving due to collisions was described in § 2. This section also described how the model could be applied to determine the properties of the disks of a population of stars, given that these disks would have had a range of initial properties. This was applied in § 3 to the population of A stars that was searched for evidence of dust emission at 24 μm by Rieke et al. (2005), and it was shown that their detection statistics as a function of age could be reproduced with a model population in which the largest planetesimals have a size of $D_c = 60$ km, and all planetesimals have a strength of $Q_D^\star = 300$ J kg^{-1} and an eccentricity of $e = 0.05$. However, these parameters should not be overinterpreted, since the observable properties of the model population remain the same as long as the combination $D_c^{0.5} Q_D^{\star 5/6} e^{-5/3}$ is unchanged. Thus, more detailed models of the collisional evolution of planetesimal belts (e.g., Krivov et al. 2005) are needed to interpret these parameters, e.g., in terms of the composition of the planetesimal belts. For now we note that these are reasonable parameters based on planetesimal (Benz & Asphaug 1999) and planet formation models (Kenyon & Bromley 2002). The model used as input a distribution of planetesimal belt starting masses that is lognormal with the same width (1 σ of 1.14 dex) inferred for protoplanetary disks (Andrews & Williams 2005), and found such a distribution would have to be centered on $M_{mid} = 10\ M_\oplus$. This mass is consistent with that expected for protoplanetary disks around A stars, although the observable properties of the model population are also reproduced as long as $M_{mid} D_c^{-0.5}$ is unchanged. In other words, the observable 24 μm properties of main-sequence A star disks can be explained by the steady state evolution of a disk population with realistic starting parameters (although more extreme solutions are also possible).

In § 4 this model was tested against its predictions for the 70 μm properties of the disks in this population. These were found to reproduce the statistics of the Su et al. (2006) survey, which showed a much longer decay timescale for the 70 μm excess than for that at 24 μm. The model was also used to predict the properties of the subsample of disks that could be detected at both 24 and 70 μm, and this was compared with a sample of 46 A stars compiled from the literature for which excess emission has been detected at both 24 and 70 μm. The model reproduces and explains the distribution of the observed disks on the f versus r (Fig. 4), f versus t_{age} (Fig. 5), and r versus t_{age} (Fig. 6) plots, including an upper envelope in the f versus r plot that increases $\propto r^{7/3}$, a decay in the mean luminosity of disks with age $\propto t_{age}^{-0.39}$, and a mean radius of detected disks that, if anything, increases with age $\propto t_{age}^{0.20}$.

Thus it appears that the wide range in typical disk properties can be explained without appealing to stochasticity. The large spread in 24 μm fractional excess at any age (Rieke et al. 2005) can occur naturally from a spread in initial disk masses and radii, and the slower falloff at 70 μm and more detailed distributions of the properties of disks detected at 24 and 70 μm (Su et al. 2006) could be the consequence of the detection bias. This bias is best explained on the plot of f versus r, on which it is possible to plot the lines above which disks must lie to be detected at 24 and 70 μm, and below which they must lie for a given age. One il-

lustrative example of this bias is the fact that while in the model the planetesimal belt of any individual star does not change in radius, the mean radius of detected planetesimal belts is predicted to increase with age. The reason is that planetesimal belts that are closest to the star are processed faster and so fall below the detection threshold much faster than planetesimal belts that are farther from the star. Thus if such a trend is seen it would not necessarily be evidence for delayed stirring, in which the collisional cascade is only initiated once enough time has elapsed for Pluto-sized objects to form, a process which takes longer farther from the star (e.g., Kenyon & Bromley 2002; Dominik & Decin 2003). Rather it could be evidence that the processing of the planetesimal belt is occurring inside-out, as inferred by Su et al. (2006).

This does not rule out the possibility that some, or even all, A star debris disks in the Rieke et al. (2005) and Su et al. (2006) samples are undergoing transient events on top of the overall trend established by the model. In fact, there are a few disks that may (rather than must) require this mechanism to explain their properties. The potentially transient systems identified in this paper are HD 3003, HD 38678, and HD 172555, which have high luminosity for their age; as well as HD 115892, which has an unusually low radius for its age. All of these systems are identifiable by their high value of f/f_{max}, where f_{max} is the maximum possible fractional luminosity that a disk can have given its age and radius (assuming the planetesimal belt properties inferred for the rest of the population). We also found that the disks of HD 2262 and HD 106591 have unusually low radii for their age, and suggested that this may be attributable to the action of PR drag on dust produced in their dust belts, since this starts to become important when $f < f_{pr}$, and these belts (along with HD 115892 and HD 19356) can be identified from the sample as having $f/f_{pr} < 1$. Neither do the results in this paper imply that the collisional cascade in all A star planetesimal belts must have been initiated soon (~10 Myr) after the stars formed, rather than the collisional cascade being initiated after a delay of several tens or hundreds of Myr in some systems (i.e., the delayed stirring model). Indeed, if the lack of large radii disks at young ages is confirmed (Rhee et al. 2007), this would support some role for delayed stirring in debris disk evolution.

Analysis of the distribution of f/f_{max} of the 46 A star disks detected at both 24 and 70 μm shows a distribution that may be attributed to the planetesimal belts not having exactly the same properties, but having a distribution in the combination of parameters given by $D_c^{0.5} Q_D^{\star 5/6} e^{-5/3}$ (which is also the combination in the parameter f_{max}) that is lognormal with a 1 σ width of 1 dex. This means two things. First, the distribution of parameters of these A stars is quite uniform. This is perhaps to be expected if the planetesimals in all belts are of similar composition, and grow to a similar maximum size before perturbations from the largest member of the cascade (around 2000 km) stir the rest of the planetesimal belt resulting in eccentricities of similar magnitude (e.g., Kenyon & Bromley 2002). Second, the anomalous systems identified in the last paragraph are only 1–2 σ anomalies in that they may be explained as disks with higher than average planetesimal strength or size, or lower than average eccentricity. In contrast, this analysis strengthens the result of Wyatt et al. (2007), in which the dust emission from several Sun-like stars, such as HD 69830, was inferred to be transient, since if the planetesimal belts of Sun-like stars are described by similar properties to those of A stars, then all of the disks they inferred to be transient have $f/f_{max} > 4000$ and each one would be a >3.6 σ anomaly (and yet such disks are

found around ∼2% of stars). However, given current limits in definitive detection of transient events, the derived incidence is probably a lower limit.

One particularly interesting outcome of the model is the distribution of radii of the planetesimal belts. The model assumed a power-law distribution of radii in the range 3–120 AU and found from the distribution of radii of the sample detected at 24 and 70 μm that this follows $N(r) \propto r^{-0.8 \pm 0.3}$. It was found to be important to take the detection bias into account when interpreting the observed distribution. The origin of this distribution is not considered in this model, which assumes that all stars have relatively narrow planetesimal belts with $dr/r = 0.5$. The inner hole in these belts has been inferred in other studies to be caused by the presence of inner planets (e.g., Roques et al. 1994; Wyatt et al. 1999; Wilner et al. 2002; Wyatt 2003; Quillen 2006). If these are Kuiper belt analogs (Wyatt et al. 2003b), then this radius distribution would be indicative of the orbital radius of the outermost planet in its planetary system. However, these could also be asteroid belt analogs, i.e., planetesimal belts in the midst of a planetary system. If so, the interpretation of this radius distribution is less clear and could, like the solar system for example, be indicative of the orbital radius of the most massive giant planet in these systems. In any case, this distribution provides an important and unique constraint on the outcome of planet formation models.

Another particularly powerful application of the model is that, regardless of the physical reason, it does explain the far-IR properties of A star disks and so it can also be used to make predictions for what surveys at other wavelengths (or with different detection thresholds) will see. Such predictions are made much easier when the survey detection threshold is uniform, or at least can be readily characterized, and this study emphasizes the importance of a characterizable threshold for future surveys. One such survey is the SCUBA-2 debris disks survey (Matthews et al. 2007), which will include an unbiased submillimeter survey of the 100 nearest A stars to a uniform 3 σ sensitivity of 2 mJy at 850 μm. The model predicts that 17 of the 100 will be detected above 2 mJy, including five above 10 mJy, and that five of the detected disks should be resolvable in submillimeter imaging on size scales >6″. However, the detected fraction could be higher than this, since it depends on the radius distribution, on which these observations would set strong constraints. It is also unknown how many A stars possess disks too cold to detect in the far-IR (Wyatt et al. 2003; Najita & Williams 2005). This suggests that the SCUBA-2 survey will be particularly fruitful, and the model presented here provides a framework which can be used to interpret the results of this survey, and those of future surveys.

REFERENCES

Absil, O., et al. 2006, A&A, 452, 237
Andrews, S. M., & Williams, J. P. 2005, ApJ, 631, 1134
Augereau, J. C., Lagrange, A. M., Mouillet, D., Papaloizou, J. C. B., & Grorod, P. A. 1999, A&A, 348, 557
Augereau, J. C., Nelson, R. P., Lagrange, A. M., Papaloizou, J. C. B., & Mouillet, D. 2001, A&A, 370, 447
Aumann, H. H., et al. 1984, ApJ, 278, L23
Beichman, C. A., et al. 2005, ApJ, 626, 1061
Benz, W., & Asphaug, E. 1999, Icarus, 142, 5
Bottke, W. F., Durda, D. D., Nesvorný, D., Jedicke, R., Morbidelli, A., Vokrouhlický, D., & Levison, H. 2005, Icarus, 175, 111
Chen, C. H., & Jura, M. 2001, ApJ, 560, L171
Chen, C. H., et al. 2006, ApJS, 166, 351
Clampin, M., et al. 2003, AJ, 126, 385
Decin, G., Dominik, C., Waters, L. B. F. M., & Waelkens, C. 2003, ApJ, 598, 636
Dent, W. R. F., Walker, H. J., Holland, W. S., & Greaves, J. S. 2000, MNRAS, 314, 702
Dermott, S. F., Jayaraman, S., Xu, Y. L., Gustafson, B. A. S., & Liou, J. C. 1994, Nature, 369, 719
Dohnanyi, J. 1969, J. Geophys. Res., 74, 2531
Dominik, C., & Decin, G. 2003, ApJ, 598, 626
Farley, K. A., Vokrouhlický, D., Bottke, W. F., & Nesvorný, D. 2006, Nature, 439, 295
Fisher, R. S., Telesco, C. M., Piña, R. K., Knacke, R. F., & Wyatt, M. C. 2000, ApJ, 532, L141
Gaidos, E. J. 1999, ApJ, 510, L131
Gomes, R., Levison, H. F., Tsiganis, K., & Morbidelli, A. 2005, Nature, 435, 466
Greaves, J. S., Fisher, D. A., Wyatt, M. C., Beichman, C. A. & Bryden, G. 2007, MNRAS, in press
Greaves, J. S., Mannings, V., & Holland, W. S. 2000, Icarus, 143, 155
Greaves, J. S., & Wyatt, M. C. 2003, MNRAS, 345, 1212
Greaves, J. S., Wyatt, M. C., Holland, W. S., & Dent, W. R. F. 2004, MNRAS, 351, L54
Habing, H. J., et al. 1999, Nature, 401, 456
Haisch, K. E., Lada, E. A., & Lada, C. J. 2001, ApJ, 553, L153
Holland, W. S., et al. 1998, Nature, 392, 788
Holmes, E. K., Butner, H. M., Fajardo-Acosta, S. B., & Rebull, L. M. 2003, AJ, 125, 3334
Kalas, P., Graham, J. R., & Clampin, M. 2005, Nature, 435, 1067
Kalas, P., & Jewitt, D. 1995, AJ, 110, 794

Kenyon, S. J., & Bromley, B. C. 2002, AJ, 123, 1757
———. 2004, AJ, 127, 513
Krivov, A. V., Sremcevic, M., & Spahn, F. 2005, Icarus, 174, 105
Lecar, M., Franklin, F. A., Holman, M. J., & Murray, N. J. 2001, ARA&A, 39, 581
Liou, J.-C., & Zook, H. A. 1999, AJ, 118, 580
Matthews, B., et al. 2007, PASP, submitted
Moerchen, M. M., Telesco, C. M., Packham, C., & Kehoe, T. J. J. 2007, ApJ, 655, L109
Moro-Martín, A., & Malhotra, R. 2003, AJ, 125, 2255
Najita, J., & Williams, J. P. 2005, ApJ, 635, 625
Natta, A., Grinin, V., & Mannings, V. 2000, in Protostars and Planets IV, ed. V. Mannings, A. P. Boss, & S. S. Russell (Tuscon: Univ. Arizona Press), 559
Nesvorný, D., Bottke, W. F., Levison, H. F., & Dones, L. 2003, ApJ, 591, 486
Quillen, A. C. 2006, MNRAS, 372, L14
Rhee, J. H., Song, I., Zuckerman, B., & McElwain, M. 2007, ApJ, 660, 1556
Rieke, G. H., et al. 2005, ApJ, 620, 1010
Roques, F., Scholl, H., Sicardy, B., & Smith, B. A. 1994, Icarus, 108, 37
Schneider, G., et al. 2006, ApJ, 650, 414
Sheret, I., Dent, W. R. F., & Wyatt, M. C. 2004, MNRAS, 348, 1282
Song, I., Caillault, J.-P., Barrado y Navascués, D., & Stauffer, J. R. 2001, ApJ, 546, 352
Song, I., Zuckerman, B., Weinberger, A. J., & Becklin, E. E. 2005, Nature, 436, 363
Spangler, C., Sargent, A. I., Silverstone, M. D., Becklin, E. E., & Zuckerman, B. 2001, ApJ, 555, 932
Stauffer, J. R., Hartmann, L. W., & Barrado y Navascues, D. 1995, ApJ, 454, 910
Stern, S. A. 1996, AJ, 112, 1203
Su, K. Y. L., et al. 2005, ApJ, 628, 487
———. 2006, ApJ, 653, 675
Telesco, C. M., et al. 2000, ApJ, 530, 329
———. 2005, Nature, 433, 133
Weinberger, A. J., Rich, R. M., Becklin, E. E., Zuckerman, B., & Matthews, K. 2000, ApJ, 544, 937
Williams, J. P., & Andrews, S. M. 2006, ApJ, 653, 1480
Wilner, D. J., Holman, M. J., Kuchner, M. J., & Ho, P. T. P. 2002, ApJ, 569, L115
Wyatt, M. C. 2003, ApJ, 598, 1321
———. 2005, A&A, 433, 1007
Wyatt, M. C., & Dent, W. R.F, 2002, MNRAS, 334, 589

Wyatt, M. C., Dent, W. R. F., & Greaves, J. S. 2003a, MNRAS, 342, 876

Wyatt, M. C., Dermott, S. F., Telesco, C. M., Fisher, R. S., Grogan, K., Holmes, E. K., & Pińa, R. K. 1999, ApJ, 527, 918

Wyatt, M. C., Greaves, J. S., Dent, W. R. F., & Coulson, I. M. 2005, ApJ, 620, 492

Wyatt, M. C., Holland, W. S., Greaves, J. S., & Dent, W. R. F. 2003b, Earth, Moon, and Planets, 92, 423

Wyatt, M. C., Smith, R., Greaves, J. S., Beichman, C. A., Bryden, G., & Lisse, C. M. 2007, ApJ, 658, 569